Impact of assimilating airborne Doppler radar velocity data using the ARPS 3DVAR on the analysis and prediction of Hurricane Ike (2008)

Ningzhu Du,[1,2] Ming Xue,[2,3,4] Kun Zhao,[2,4] and Jinzhong Min[1]

Received 24 February 2012; revised 1 August 2012; accepted 3 August 2012; published 25 September 2012.

[1] The ARPS 3DVAR data assimilation system is enhanced and used for the first time to assimilate airborne Doppler radar wind observations. It is applied to Hurricane Ike (2008), where radar observations taken along four flight legs through the hurricane vortex 14 to 18 h before it made landfall are assimilated. An optimal horizontal de-correlation scale for the background error is determined through sensitivity experiments. A comparison is made between assimilating retrieved winds and assimilating radial velocity data directly. The effect of the number of assimilation cycles, each analyzing data from one flight leg, is also examined. The assimilation of retrieved wind data and of radial velocity data produces similar results. However, direct assimilation of radial velocity data is recommended for both theoretical and practical reasons. In both cases, velocity data assimilation improves the analyzed hurricane structure and intensity as well as leads to better prediction of the intensity. Improvement to the track forecasting is also found. The assimilation of radial velocity observations from all four flight legs through intermittent assimilation cycles produces the best analyses and forecasts. The first analysis in the first cycle tends to produce the largest analysis increment. It is through the mutual adjustments among model variables during the forecast periods that a balanced vortex with lowered central pressure is established. The wind speeds extracted from the assimilated model state agree very well with independent surface wind measurements by the stepped-frequency microwave radiometer onboard the aircraft, and with independent flight-level wind speeds detected by the NOAA P-3 aircraft in-flight measurements. Twenty-four hour accumulated precipitation is noticeably improved over the case without radar data assimilation.

Citation: Du, N., M. Xue, K. Zhao, and J. Min (2012), Impact of assimilating airborne Doppler radar velocity data using the ARPS 3DVAR on the analysis and prediction of Hurricane Ike (2008), *J. Geophys. Res.*, *117*, D18113, doi:10.1029/2012JD017687.

1. Introduction

[2] A hurricane is one of the most intense forms of natural disaster. Accurate predictions of a hurricane's track, intensity and structure near its landfall are crucial for the protection of life and property in coastal regions. Significant improvement has been made for hurricane track forecasting in the past two decades, but the prediction of hurricane intensity has seen much less improvement [*Elsberry*, 2005; *Houze et al.*, 2007; *Davis et al.*, 2008]. As pointed out by *Houze et al.* [2007], intensity prediction depends heavily on the inner-core vortex dynamic and thermodynamic structures and their evolutions; obtaining accurate analyses of the inner-core structures is therefore important.

[3] Toward that goal, observational data with high temporal and spatial resolutions in the hurricane inner-core region are needed. Conventional observations are too sparse, particularly over the ocean, to measure the hurricane's inner core. Most satellite data over the hurricane inner-core area are contaminated by heavy precipitation. Doppler weather radar becomes the only available platform that can provide such observations. However, the measurement parameters are limited to the radial velocity (Vr) and reflectivity (Z), which are not model state variables. This makes it necessary to use advanced data assimilation methods capable of 'retrieving' state variables not directly observed.

[1]Jiangsu Key Laboratory of Meteorological Disaster, Nanjing University of Information Science and Technology, Nanjing, China.
[2]Center for Analysis and Prediction of Storms, University of Oklahoma, Norman, Oklahoma, USA.
[3]School of Meteorology, University of Oklahoma, Norman, Oklahoma, USA.
[4]Key Laboratory of Mesoscale Severe Weather/Ministry of Education, China School of Atmospheric Sciences, Nanjing University, Nanjing, China.

Corresponding author: M. Xue, Center for Analysis and Prediction of Storms, University of Oklahoma, 120 David L. Boren Blvd., Norman, OK 73072, USA. (mxue@ou.edu)

0148-0227/12/2012JD017687

[4] Studies have shown that hurricane inner-core structures can be analyzed from either ground-based or airborne Doppler radar (ADR) data [e.g., *Blackwell*, 2000; *Marks and Houze*, 1984, 1987; *Reasor et al.*, 2000; *Gamache*, 2005]. Studies that assimilate Doppler radar data into numerical weather prediction (NWP) models did not start to appear until recent years. *Xiao et al.* [2007] showed that assimilating reflectivity data from one coastal radar using a 3DVAR system improved inland forecasting of a landfalling typhoon. Their study used a 3-hourly assimilation cycle that is considered long compared to the radar volume scan interval. *Zhao and Jin* [2008] assimilated coastal WSR-88D radar radial velocity and reflectivity data within the landfall region of Hurricane Isabel (2003) into the Navy's Coupled Ocean/Atmosphere Mesoscale Prediction System (COAMPS), using the COAMPS 3DVAR system. Their results indicated positive impacts of radar data on the hurricane vortex initialization, and on the structure, intensity and precipitation forecasts. *Xiao et al.* [2009] assimilated reflectivity data and winds pre-retrieved from radial velocity data of a radar onboard the NOAA P-3 reconnaissance aircraft for Hurricane Jeanne (2004), Katrina (2005) and Rita (2005) during their rapid intensification and subsequent weakening phases near landfall. The WRF [*Skamarock et al.*, 2005] 3DVAR system was used with a single time analysis. Their study concluded that the assimilation of the ADR data improved the analysis of hurricane vortex structures and the subsequent intensity forecasts. Using the same WRF 3DVAR system, *Pu et al.* [2009] also assimilated ADR retrieved wind and reflectivity data for Hurricane Dennis (2005). The findings showed that the assimilation of reflectivity data had a notable influence on the thermal and hydrometeor structures of the initial vortex and on the precipitation structure in the subsequent forecasts, while the assimilation of radar wind data resulted in significant improvement in the intensity and precipitation forecasts. The hurricane intensification, landfall, and weakening during the simulation period were better captured when both reflectivity and wind data were assimilated.

[5] Both *Xiao et al.* [2009] and *Pu et al.* [2009] analyzed, at a single time, the ADR wind data pre-retrieved into the horizontal wind components on regular Cartesian coordinates using a separate 3DVAR procedure [*Gamache*, 2005]. Using the ensemble Kalman filter (EnKF) method, *Zhang et al.* [2011] assimilated ADR radial velocity data directly for hurricane forecasts using the WRF model at a convection permitting resolution. By assimilating data from over 60 NOAA P-3 airborne Doppler radar measurement missions from the 2008–2010 Atlantic hurricane seasons, they showed the promise of ADR radial velocity data for improving hurricane intensity forecasts. Using the same system, *Weng and Zhang* [2012] documented the positive impacts of airborne Doppler radar winds on the prediction of Hurricane Katrina (2005).

[6] Despite the studies cited above, the assimilation of airborne Doppler radar data into an NWP model for tropical cyclone forecasts is still at a stage of infancy. The first two studies cited used the WRF 3DVAR system with a single time analysis of pre-retrieved wind data while the latter two used the more sophisticated EnKF method to assimilate radial velocity data directly at hourly intervals for a couple of times. All four studies used the Advanced Research WRF model. A more recent study by *Li et al.* [2012] has documented issues with the WRF 3DVAR analysis of radial velocity data using the typical static background error covariance, which would also prevent the use of short assimilation cycles. Clearly, research on the airborne radar data assimilation and investigation of alternative methods, for different tropical cyclone cases, is still needed to further improve the assimilation performance and document the general impacts of the ADR velocity data. In this study, Hurricane Ike (2008) is used as a testbed for examining the impacts of ADR velocity data when assimilated using a 3DVAR method.

[7] Recently, *Zhao and Xue* [2009] applied the 3DVAR and cloud analysis system of the Advanced Regional Prediction System (ARPS) [*Xue et al.*, 2003; *Gao et al.*, 2004; *Hu et al.*, 2006a] to assimilate observations from two coastal ground-based WSR-88D radars for landfalling Hurricane Ike (2008). In the study, radial velocity and reflectivity were assimilated over a 6 h period before Ike's landfall, at 30 min intervals. All experiments that assimilated radial velocity and/or reflectivity data produced better structure, intensity and precipitation forecasts than those from operational GFS analysis. The radial velocity data were found to help improve the track forecast more while reflectivity data helped improve intensity forecast most. The best results were obtained when both radial velocity and reflectivity data were assimilated. The ARPS 3DVAR system was developed specifically with assimilation of high-frequency radar data in mind [e.g., *Hu and Xue*, 2007] while the study by *Zhao and Xue* [2009] was the first successful application of the system to a hurricane case. A more recent study by *Zhao et al.* [2012b] documents further success in applying the system to a Pacific typhoon case. This system has not been applied to airborne Doppler radar data, however. The EnKF method is theoretically more advanced. However, it costs much higher computational resources. Therefore, the performance of the much cheaper 3DVAR method is still worth being investigated.

[8] In this study the APRS 3DVAR system is enhanced to be able to assimilate airborne Doppler radar radial velocity data. Hurricane Ike (2008) is chosen as the test case because of the availability of the airborne radar data one to two days prior to its landfall and the same case was used in *Zhao and Xue* [2009], which assimilated coastal radar data. Two types of radar wind data are tested. One is composed of pre-retrieved wind components produced by the Hurricane Research Division (HRD) of AOML (Atlantic Oceanographic & Meteorological Laboratory) in real time [*Gamache et al.*, 2004; *Gamache*, 2005], and the other is the radial velocity data before any retrieval (referred to as Vr). The former was the type used in *Xiao et al.* [2009] and *Pu et al.* [2009]. The relative performance of the two types of data will be compared. We will examine the ability of these data in producing realistic internal structures of hurricane vortices, the effects of the 3DVAR configurations, including the spatial correlation scales of the background error covariance and the number of assimilation cycles. Verifications against independent in situ and remotely sensed observations in the inner-core region will be made, and the impacts of the radar data assimilation on the subsequent forecast of Ike will be examined.

[9] The rest of this paper is organized as follows. In section 2, a brief review of Hurricane Ike and the ADR observations are given. The methodology for assimilating the ADR wind data and the experimental design are described in section 3.

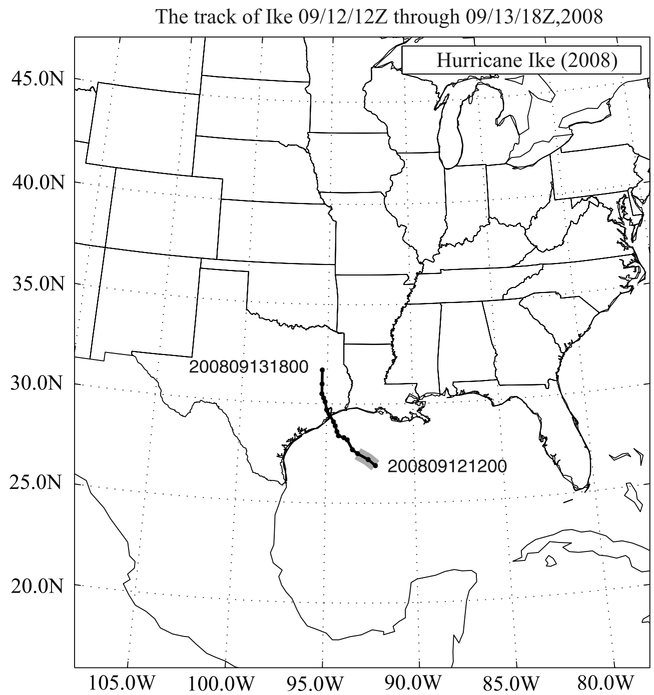

Figure 1. The hurricane analysis and forecast domain used and the observed (best track) positions (black solid line) of Hurricane Ike from 1200 UTC 12 September to 1800 UTC 13 September, 2008. The shaded gray segment of the track corresponds to the period of 4 data assimilation cycles in this study. Hurricane center positions are plotted at times best track data are available. The intervals between best track data are uneven.

Sections 4 and 5 present the results while the summary and conclusions are provided in section 6.

2. Hurricane Ike (2008) and Airborne Doppler Radar Data

2.1. A Brief Depiction of Hurricane Ike (2008)

[10] Hurricane Ike started as a tropical disturbance off the west coast of Africa near the end of August, 2008. It was the third most destructive Atlantic hurricane on record to make landfall in the United States, after Hurricanes Andrew (1992) and Katrina (2005). According to *Berg* [2009], when Ike moved west-northwestward over the tropical Atlantic, it strengthened and became a tropical storm on 1 September. It further intensified to hurricane strength on 3 September, and then rapidly reached its peak intensity of Category 4, with the maximum sustained wind speed reaching 64 m s^{-1} on 4 September. In the next few days, Ike weakened and temporarily fell below major hurricane status after passing over Great Inagua in the Bahamas, but then rapidly intensified to Category 4 strength again over a 6 h period as deep convection redeveloped in its northern semicircle. After that, it weakened, after passing near and over Cuba, and moved into the Gulf of Mexico. Over the Gulf of Mexico, Ike moved slowly northwestward with maximum sustained winds strengthening to 43 m s^{-1} on 10 September. It moved west-northwestward again later on 10 September, accompanied by an eyewall replacement phenomenon: the contraction of the outer eyewall occurred, the inner eyewall dissipated, and finally the contracted outer eyewall became the more dominant feature by 1800 UTC 11 September. Therefore, Ike lost some of its inner core convection and a large wind field developed on 12 September. These circumstances made it difficult to intensify rapidly. At 0700 UTC 13 September, Ike turned to the north-northwest and made landfall, as Category 2 strength, along the north end of Galveston Island, Texas. It weakened to a tropical storm by 1800 UTC 13 September.

[11] This study focuses on the time period of near landfall from 1200 UTC 12 September to 1800 UTC 13 September, 2008 (Figure 1). There are two reasons for this selection: first, the prediction of hurricanes near landfall is of great importance and has direct influence on human lives and properties along coastal regions; second, ADR data are available between 1200 UTC and 1800 UTC 12 September.

2.2. A Brief Description of Airborne Doppler Radar Velocity Data

[12] The airborne Doppler radar data used in this study were gathered by the NOAA 43RF aircraft which participated in an Environmental Modeling Center (EMC) Tail Doppler Radar mission. The radar operated at the X-band. The retrieved velocity data we used are the horizontal wind components, derived by HRD from radial velocity data using a 3DVAR technique after automatic quality control including sea clutter and noise removal and velocity de-aliasing [*Gamache*, 2005]. The 3DVAR retrieval algorithm used is similar to the one documented in *Gao et al.* [1999] which is also the basis of the ARPS 3DVAR [*Gao et al.*, 2004]. Since the retrieved velocity data are already the horizontal wind components, they can be assimilated like conventional observations without any special observation operator. While they are much easier to use in realtime applications, the pre-retrieval step does consume valuable time. In the data assimilation field, it is generally preferable to directly assimilate the original form of observations whenever possible. The pre-retrieval step can also introduce error correlation among the retrieved data, which is difficult to characterize while data assimilation systems commonly assume the observation errors are uncorrelated. Further, the pre-retrieval procedure is often less optimal than the full data assimilation procedure where information from all sources is considered together. It is therefore worthwhile to compare the relative performance of directly assimilating Vr data to the assimilation of retrieved wind data; this is done in this study.

[13] Figure 2 shows the horizontal distributions of the ADR radial velocity data aggregated from all levels for the four flight legs. The time periods of those flight legs are 1235 to 1329 UTC, 1358 to 1451 UTC, 1511 to 1558 UTC, and 1621 to 1715 UTC 12 September, 2008, respectively. The flights passed through the vortex center at 1308, 1420, 1540 and 1640 UTC, respectively. Before assimilating the ADR radial velocity data, a pre-processing procedure is applied. The observations are thinned along each radar beam. Because the model horizontal grid spacing is 4 km and the gate space is 150 m along the radar beams, radial velocity data of every 30 gates are averaged along each beam to give 'superobs' of about 4.5 km intervals giving a radial resolution similar to that of model grid. The processed data remain on the radar beams and are directly analyzed by the 3DVAR as such. Because the airborne radar is constantly moving, radar

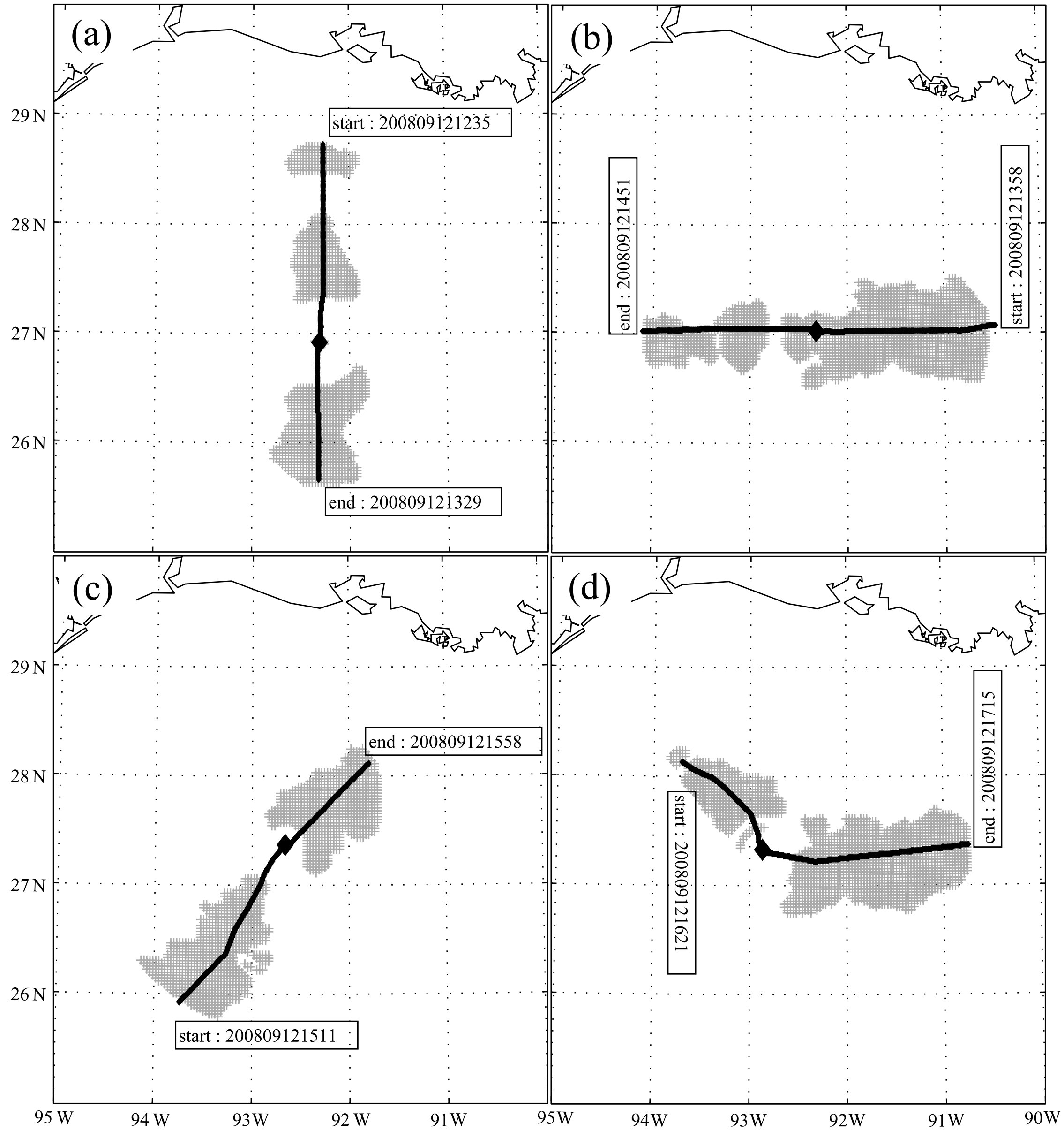

Figure 2. Horizontal distributions of airborne Doppler radar radial velocity observations aggregated from all levels for Hurricane Ike at four flight legs: (a) 1235–1329 UTC, (b) 1358–1451 UTC, (c) 1511–1558 UTC, and (d) 1621 to 1715 UTC, 12 September, 2008. The black filled diamond stands for vortex center recorded at 1308, 1420, 1540 and 1640 UTC, and the thick black line in each panel indicates the flight track.

locations coded with individual beams are used in the radial velocity observation operator that interpolates the model velocity to the superob locations then projects it to the radial direction. In comparison, for ground-based radar data, the ARPS 3DVAR system uses radial velocity data that have been mapped to the model grid points in the pre-processing step [*Brewster et al.*, 2005; *Hu et al.*, 2006b].

[14] In our experiments, radial velocity data collected within each flight leg are considered to be valid and analyzed by the 3DVAR at the time when the flight passed the hurricane center. Figure 3 shows, as an example, the vertical distribution of the number of radial velocity data of the first flight leg, from 1235 to 1329 UTC (Figure 2a). The vertical distributions for the other three times are similar. As can be seen, most data are found between 1 to 10 km, and the majority is between 1 and 4 km.

3. Assimilation Methodology and Experiment Design

3.1. ARPS Model Domain and Configurations

[15] The numerical model used in this study is ARPS, a multipurpose, three-dimensional, non-hydrostatic, and compressible NWP model developed by the Center for Analysis and Prediction of Storms (CAPS), the University of Oklahoma [*Xue et al.*, 2000, 2001, 2003]. As in *Zhao and Xue* [2009], the general physics configurations for all experiments in this study include the Lin six-class microphysics

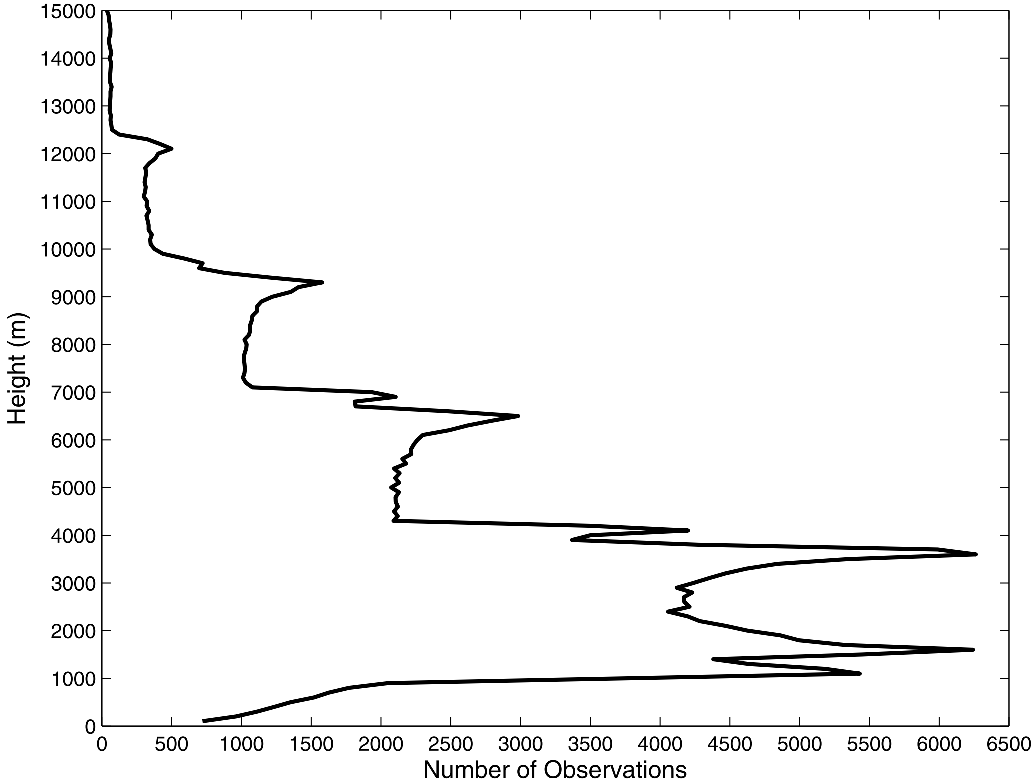

Figure 3. Vertical profile of the number of airborne Doppler radar radial velocity observations at 1308 UTC 12 September, 2008.

scheme [*Lin et al.*, 1983], Goddard longwave and shortwave radiation schemes, a 2-layer soil model, and the 1.5-order TKE-based subgrid-scale turbulence mixing PBL parameterization. The numerics used include fourth-order advection in both horizontal and vertical, a rigid top boundary condition combined with a wave absorbing layer, and fourth-order computational mixing. A more detailed description of these options can be found in *Xue et al.* [2000; 2001]. The lateral boundary conditions (LBCs) are provided from 6-hourly NCEP GFS analyses combined with 3 h GFS forecasts at 0.5° resolution.

[16] A model domain with a 4 km horizontal grid spacing is used for this study (Figure 1). The grid dimensions are $803 \times 883 \times 53$ in the east–west, north–south, and vertical directions, respectively. The grid is stretched in the vertical, with a minimum vertical grid spacing of 50 m near the surface and an average vertical resolution of 0.5 km. Grid stretching is calculated according to a hyperbolic tangent function of height [*Xue et al.*, 1995]. The physical domain centered at 32.50°N, 93°W is 3200 km × 3520 km × 25 km, covering the entire circulation of Ike as well as its surrounding environment for the analysis and forecast period. The initial background in all experiments is from the 0.5° NCEP GFS operational analysis at 1200 UTC 12 September, 2008.

3.2. The ARPS 3DVAR Analysis System

[17] The ARPS 3DVAR utilizes an incremental form of the cost function that includes the background, observation and equation constraint terms. The three wind components, u, v, and w are used directly as the control variables [*Gao et al.*, 2004] and they are directly updated by the 3DVAR when analyzing radial velocity data. Because the airborne data remain on the radar beams, the radial velocity observation operator includes first an interpolation of model wind components to the observation location then the projection of the velocity to the radial direction. The latter is the same as that used for ground-based radar data in the ARPS 3DVAR, except that the radar location changes with each beam. When assimilating the retrieved velocity data, which are the two horizontal wind components already, they are treated like convectional data in the ARPS 3DVAR.

[18] The analysis increments are obtained by minimizing the 3DVAR cost function. The background error covariance assumes Gaussian spatial correlation but neglects cross-correlations between variables. The Gaussian spatial covariance is modeled by a recursive filter. The observation errors are assumed to be uncorrelated resulting in a diagonal matrix for the observation error covariance. Following *Xiao et al.* [2009] and *Pu et al.* [2009], the observational error for retrieved horizontal wind data and ADR radial velocity data is empirically set as 2.0 m s^{-1}. A weak anelastic mass continuity constraint is imposed on the wind field to link up the wind components and ensure mass continuity [*Gao et al.*, 2004]. The ARPS 3DVAR allows for the use of different spatial error de-correlation scales for different types of observations and the correlation scales are usually chosen based on the density of observational network. In this study, we perform a set of experiments to determine the optimal horizontal correlation scale for our data set and application.

Table 1. List of Experiments[a]

Group	Experiment	Radar Data	Horizontal De-correlation Scale (km)	Assimilation Cycles	24 h Mean Track Error (km)	24 h Mean minSLP Error (hPa)	24 h Mean MSW Error (m s^{-1})
Control	CTRL	None	N.A.	N.A.	26.0	15.1	8.3
Group 1	VrC4S10	Vr	10	4	23.3	11.5	8.4
	VrC4S40	Vr	40	4	17.8	9.2	8.2
	VrC4S60	Vr	60	4	20.9	8.8	7.6
	VrC4S80	Vr	80	4	26.1	9.8	8.1
	VrC4S100	Vr	100	4	24.8	8.6	8.1
	VrC4S120	Vr	120	4	25.9	7.4	8.6
	VrC4S140	Vr	140	4	43.8	8.8	10.5
Group 2	ReC4S40	Retrieved	40	4	18.7	8.7	8.2
Group 3	VrC1S40	Vr	40	1	25.2	12.8	8.3
	VrC2S40	Vr	40	2	22.2	10.3	8.6
	VrC3S40	Vr	40	3	18.9	9.9	8.2

[a]Group 1 for examining different horizontal de-correlation scales, Group 2 for comparing assimilations of Vr and retrieved wind data, and Group 3 for investigating the impacts of assimilation cycles. The last three columns list the mean track, minimum sea level pressure, and maximum surface wind speed errors, respectively, of the 24 h forecasts counting from 1800 UTC 12 September, 2008.

3.3. Design of Experiments

[19] As mentioned above, in the ARPS 3DVAR, the selection of a spatial de-correlation scale of the Gaussian background error covariance is empirically guided by the density of observational data [*Hu et al.*, 2006b; *Schenkman et al.*, 2011]. As pointed out in *Kalnay* [2002], the spatial background error covariance acts to spread observation information in space in data sparse areas and to smooth observation information in data dense areas. When the spatial coverage of an observation network is relatively uniform, the optimal choice of the scale is usually several times the mean spacing of observations. In this way, detailed structures in the observation data are not smoothed too much while a reasonable amount of spatial spreading is achieved to fill data holes and to allow for cancellation of errors in nearby observations. In fact, in the ARPS 3DVAR, multiple passes are often used as a practical measure to analyze observations from networks of very different mean spacings. A more detailed discussion on these aspects of the ARPS 3DVAR can be found in *Schenkman et al.* [2011, section 3b].

[20] In the case of ADR data, the situation is more complicated: the radar observations have high spatial density where there is data coverage but the spatial coverage of data is incomplete or spatially inhomogeneous (Figure 2). A spatial correlation scale comparable to the data resolution allows for the retention of convective-scale structures but may not be able to represent the vortex scale structures well. For hurricane initialization, proper analysis of the vortex scale structures is of first order importance. To determine the optimal spatial correlation scale, a set of experiments is first performed where the horizontal de-correlation scale (HDS) is varied from 10 to 140 km (see Group 1 in Table 1). This set of experiments assimilates Vr data from all 4 flight legs in 4 assimilation cycles, with analyses occurring at 1308, 1420, 1540, and 1640 UTC 12 September, 2008, respectively, corresponding to AC4 in Figure 4. In all experiments presented in this paper, the vertical de-correlation scale used is 4 grid levels.

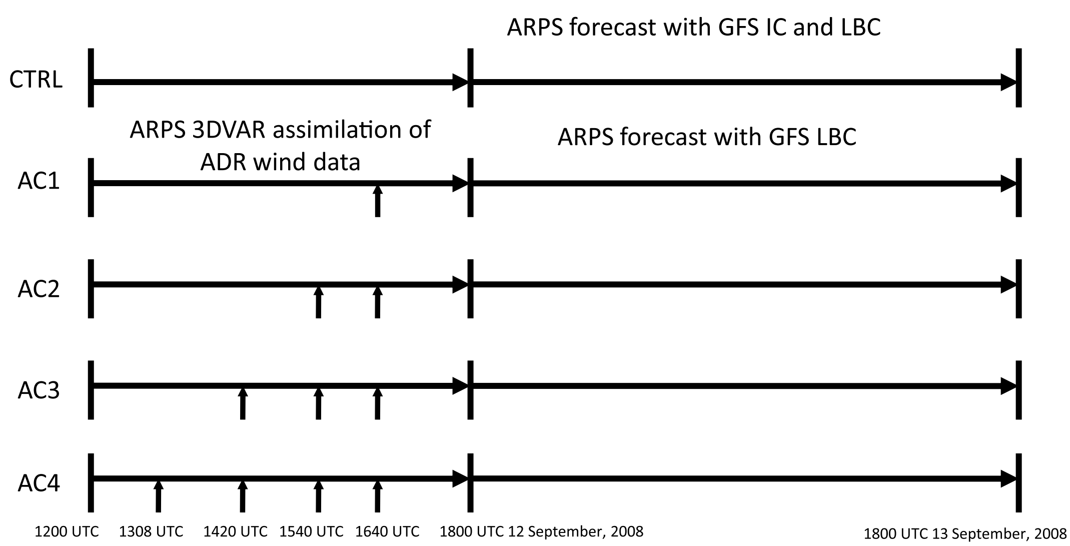

Figure 4. Flowchart of CTRL and data assimilation experiments. The upward arrows indicate the times when the radar data are assimilated. A 25 h 20 min forecast follows the last analysis at 1640 UTC in the data assimilation experiments. AC1, AC2, AC3 and AC4 stand for the use of 1, 2, 3 and 4 assimilation cycles, respectively.

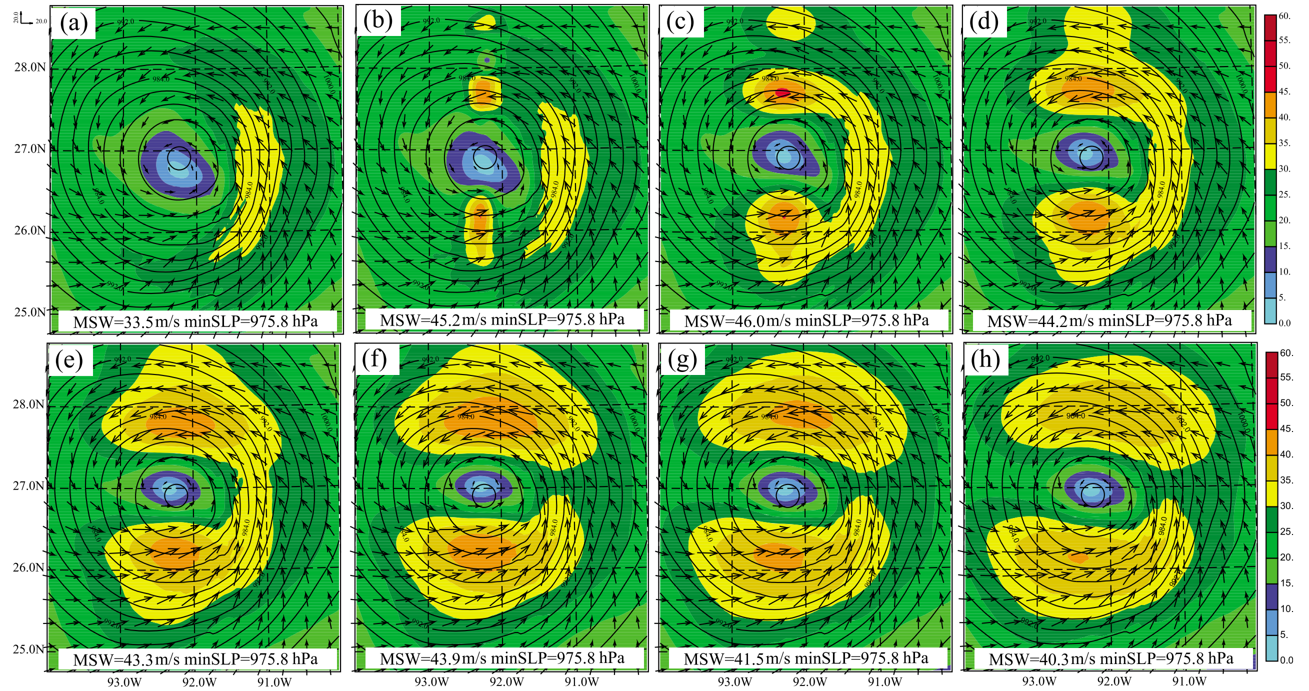

Figure 5. Surface (25 m AGL) wind vectors and wind speed (shaded contours at 5 m s^{-1} intervals), and SLP (thick contours at 2 hPa intervals) for Hurricane Ike at 1308 UTC 12 September, 2008 after the first 3DVAR analysis, for experiments (a) CTRL, (b) VrC4S10, (c) VrC4S40, (d) VrC4S60, (e) VrC4S80, (f) VrC4S100, (g) VrC4S120, and (h) VrC4S140.

[21] The second group has only one new experiment, ReC4S40, which is the same as VrC4S40 in the first group, except for the use of retrieved winds instead of Vr data. The 40 km HDS used is found to be optimal by the first group of experiments. ReC4S40 and VrC4S40 are compared to determine the relative performance of assimilating the two types of data.

[22] The third group of experiments tries to investigate the roles and effects of assimilation cycles. The assimilation setups of these experiments (Group 3 in Table 1) are the same as those of VrC4S40 except for the number of assimilation cycles (AC) performed. As shown in Figure 4, the experiments labeled C1 through C4 contain 1 to 4 assimilation cycles and the final analysis of all experiments is valid at 1640 UTC 12 September, the central time of the last flight leg. In addition, a pure forecast control experiment (CTRL) is performed, which starts from 0.5° NCEP GFS operational analysis at 1200 UTC 12 September 2008 without assimilating any radar observation. The forecasts in all experiments continue until 1800 UTC 13 September (Figure 4).

4. Impact of Data Assimilation Configurations on the Analysis and Forecast of Ike

[23] The impacts of assimilating ADR wind data on the analysis and prediction of Hurricane Ike (2008) are presented in this section. Three subsections examine, respectively, the optimal HDS for the background error covariance, the performance of assimilating retrieved wind versus that of assimilating Vr data, and the impact of the number of assimilation cycles.

4.1. Effects of Horizontal De-correlation Scale (HDS)

[24] We first discuss the results of the first group of experiments designed to determine the optimal HDS of the background error covariance model. Figure 5 shows the sea level pressure (SLP) and the wind vectors and speed at the first model level above ground (25 m AGL), within the hurricane vortex region after the first 3DVAR analysis at 1308 UTC 12 September (Figures 5b–5h) together with the corresponding CTRL forecast (Figure 5a). This CTRL forecast is also the background used by the analyses. For this analysis time, the flight track is in the north–south direction, therefore available Vr data are concentrated south and north of the vortex center (Figure 2a).

[25] As documented in *Berg* [2009], at 1200 UTC 12 September, the closest time to the first analysis when best track data are available, the minimum central sea level pressure (minSLP) and the maximum surface wind speed (MSW) are 954 hPa and 46.3 m s^{-1}, respectively. In all data assimilation experiments, MSW is increased from the ~33.5 m s^{-1} in the background (Figure 5a) to above 40 m s^{-1} after analysis (Figures 5b–5h). The increase is the largest in VrC4S40 (46 m s^{-1}, Figure 5c) and the smallest in VrC4S140 (40.3 m s^{-1}, Figure 5h). In general, the wind increment expands in area coverage and the maximum increment decreases as the HDS increases. If one were to assimilate the radial velocity data only once, one might expect that a larger HDS would work better because the data are expected to have a larger impact on the vortex strength. When additional observations are available that provide coverage in other parts of the vortex, one may want to limit the spatial influence of data to smaller regions to retain more asymmetric structures contained in the

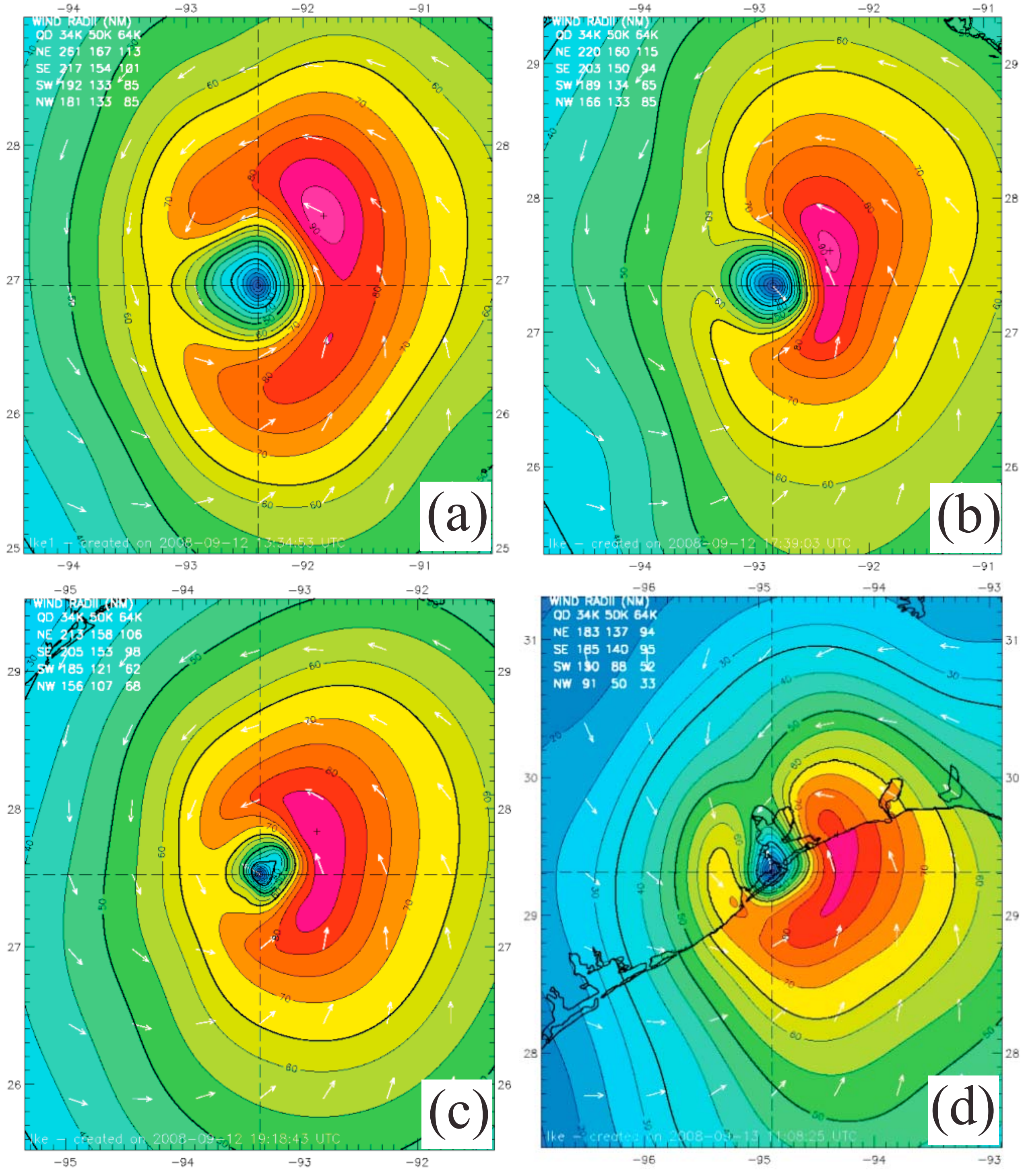

Figure 6. H*WIND isotach analysis (kt) (a) at 1330 UTC, (b) at 1630 UTC, (c) 1930 UTC 12 September, and (d) at 0730 UTC 13 September, 2008 for Hurricane Ike (from the NOAA/AOML/HRD Web site).

data. Overall, among these experiments in the first Group as listed in Table 1, the MSW in VrC4S40 is closest to the observed MSW at 1308 UTC 12 September, after the first analysis cycle. Because the cross-correlations between variables are not included in the background error covariance in the ARPS 3DVAR, the minSLP is not changed by the analysis. The change to the pressure field will be achieved through adjustments during the model integration, which occur when assimilation cycles are employed. In other words, Vr data can modify the pressure field indirectly through model adjustments during the assimilation cycles.

[26] Figure 6a shows a HRD H*WIND analysis valid at 1330 UTC 12 September, the nearest time to 1308 UTC when such an analysis is available. The H*WIND analysis

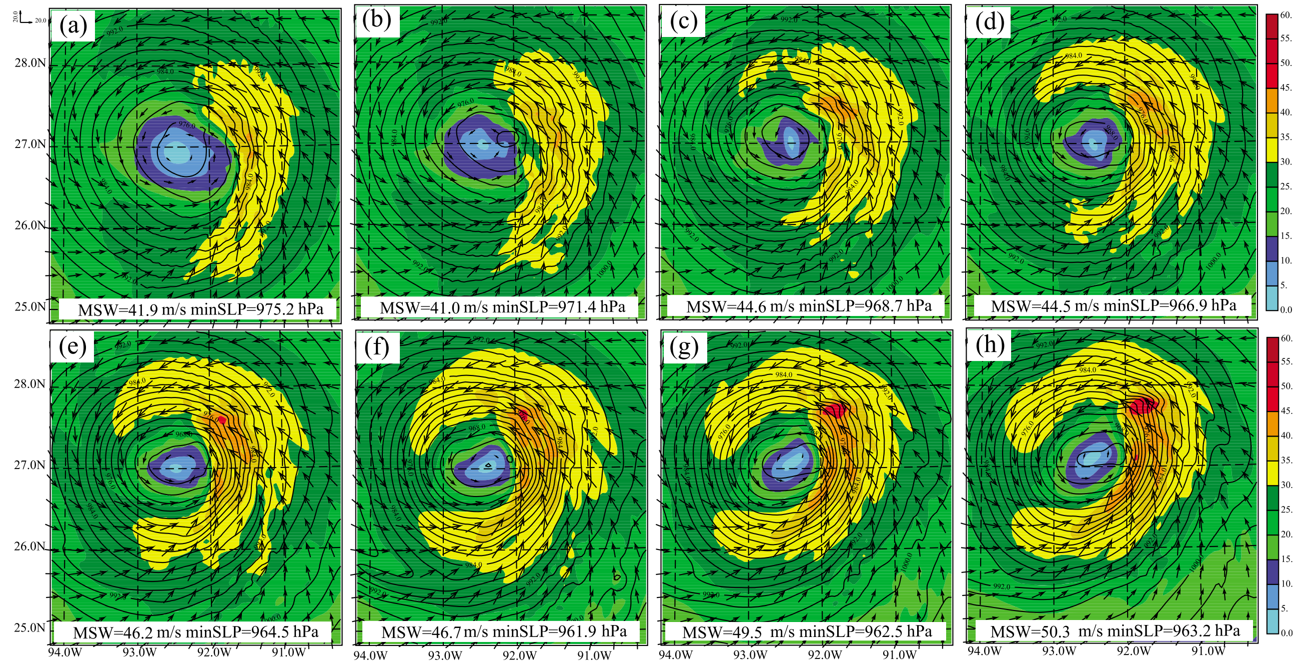

Figure 7. As Figure 5, for experiments (a) CTRL, (b) VrC4S10, (c) VrC4S40, (d) VrC4S60, (e) VrC4S80, (f) VrC4S100, (g) VrC4S120, and (h) VrC4S140, but at 1420 UTC, 12 September, 2008 before the second analysis.

combines data from reconnaissance aircraft, dropsondes, satellite-derived winds, in situ observations, and stepped-frequency microwave radiometer retrievals, and produces a gridded storm-centered 10 m, 1 min, marine exposure sustained wind field [*Powell et al.*, 1998; *Uhlhorn and Black*, 2003]. The H*WIND analysis shows that the surface maximum wind is located northeast of the vortex center, rather than the north and south found in the analyses (Figures 5b–5h). These displaced maxima are simply artifacts of the Vr data coverage (Figure 2a). The forecast background places the surface maximum wind speed east of the vortex center, which is not correct either (Figure 5a); the maximum wind speed is also too low.

[27] Figure 7 shows the fields as in Figure 5 but for forecasts starting from the analyses shown in Figure 5, and valid at 1420 UTC 12 September right before the second analysis. The forecast MSW in CTRL (Figure 7a) is again east of the vortex center, not matching the H*WIND analysis (Figure 6a). In all data assimilation experiments, the MSW north of the vortex center (Figures 5b–5h) has moved westward and lost its clear identity (Figures 7b–7h), whereas the MSW south of the vortex center (Figures 5b–5h) has propagated around the center and established itself northeast of the center while maintaining the maximum speed above 45 m s^{-1} (Figures 7b–7h). This structure is much closer to that seen in the H*WIND analysis (Figure 6a).

[28] In response to the wind analysis, the minSLP in the model decreases from 975.8 hPa (Figure 5a) at the first analysis time to below 971.4 hPa (Figures 7b–7h) before the second analysis in all data assimilation experiments. The decrease is the largest in VrC4S140 (963.2 hPa, Figure 7h), and the smallest in VrC4S10 (971.4 hPa, Figure 7b). In contrast, the minSLP in CTRL remains about the same ($\sim$975 hPa) in the 1 h 12 min forecast period (Figure 5a and Figure 7a). These results indicate the ability of Vr assimilation to improve the vortex structure and pressure forecast even though the Vr data coverage is rather asymmetric and incomplete. Figure 8 shows the MSW and minSLP during the assimilation cycles for the first group of experiments. It can be seen that the analysis of Vr data increases MSW by at least 7 m s^{-1} at each cycle in all experiments, and MSW tends to increase further during the forecast following the first analysis, but decreases in other cycles. Overall, MSW shows an increasing trend through the cycles. minSLP is not directly affected by the analysis but generally decreases through the cycles by responding to the improved wind circulations.

[29] Figure 9 presents the wind vector analysis increments at the 3.5 km height for experiments VrC4S40 and VrC4S100 at the first and second analysis cycles. This level is where the largest number of observations is available (Figure 3). When the Vr data are analyzed for the first time, the wind vector increments for all experiments in Group 1 show a clear cyclonic circulation pattern (Figures 9a and 9c). The increments of those experiments with HDS less than 100 km in Group 1 are similar to those of VrC4S40, while those with HDS larger than 100 km are similar to those of VrC4S100 (not shown). In contrast to VrC4S40 (Figure 9a), the wind vector increments in VrC4S100 (Figure 9c) cover the entire vortex due to the larger spatial influence of data located south and north of the vortex center. The increments east and west of the vortex center are established largely due to the mass continuity constraint in the ARPS 3DVAR, in connection with the large areas of increased wind speed to the south and north. In comparison, the increments in VrC4S40 are mainly limited to the north and south of the vortex center, where observations are available. The patterns of wind vector increments of the second analysis are very different (Figure 9b and Figure 9d). The increments in Figure 9b indicate that the vortex circulation

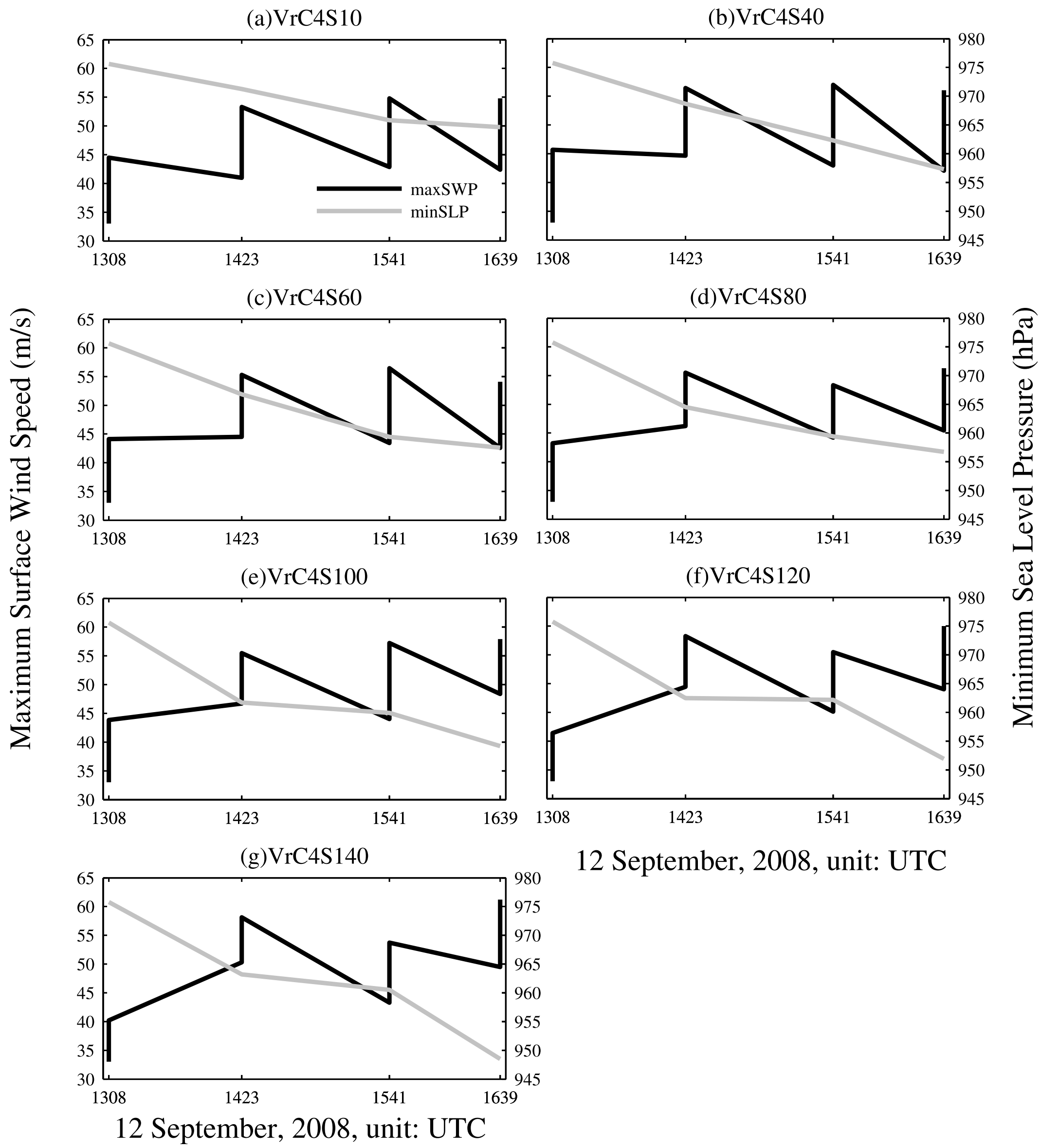

Figure 8. The analyzed and forecast maximum surface wind speed (dark) and minimum sea level pressure (gray, forecast only) during the assimilation cycles for the experiments labeled.

is still strengthened by Vr data assimilation in VrC4S40, but is weakened in VrC4S100 (Figure 9d). This suggests that the vortex was over-strengthened in VrC4S100, so the analysis tries to weaken it. For VrC4S40, the last two assimilation cycles continue to enhance the vortex as the first two cycles do. In VrC4S100, the four assimilation cycles cause an oscillatory effect: the first and third (not shown) cycles enhance the vortex while the other two weaken the vortex, suggesting that the 100 km DHS is too large.

[30] The 24 h mean forecast track and intensity errors (in both minSLP and MSW) for CTRL and Group 1 experiments with HDS less than 100 km are shown in Table 1. It is seen that VrC4S40 with 40 km HDS gives the smallest mean track error of 17.8 km, while its minSLP error is the second smallest (8.8 hPa). Table 1 shows that the relative sizes of MSW error are not always consistent with those of minSLP error; we choose to trust minSLP more because the analysis of high-resolution velocity data can easily introduce highly localized maximum wind speed that does not necessarily represent well the overall vortex intensity. Still, the overall trend of wind assimilation impact is still seen in terms of the MSW error.

[31] Based on the above results, we choose 40 km as the optimal HDS for use in the rest of the experiments. We do note here that this optimal HDS of 40 km may be case and grid resolution dependent. In general, they are dependent on the observation density and spatial distribution, as well as the error characteristics of the analysis background which should be related to the hurricane structures. Experimentations may be needed to determine the optimal scale for individual cases.

4.2. Assimilating Vr Versus Retrieved Velocity Data

[32] In this section, we compare the results of assimilating retrieved wind data versus assimilating Vr data directly. The 40 km optimal HDS is also used in the experiment

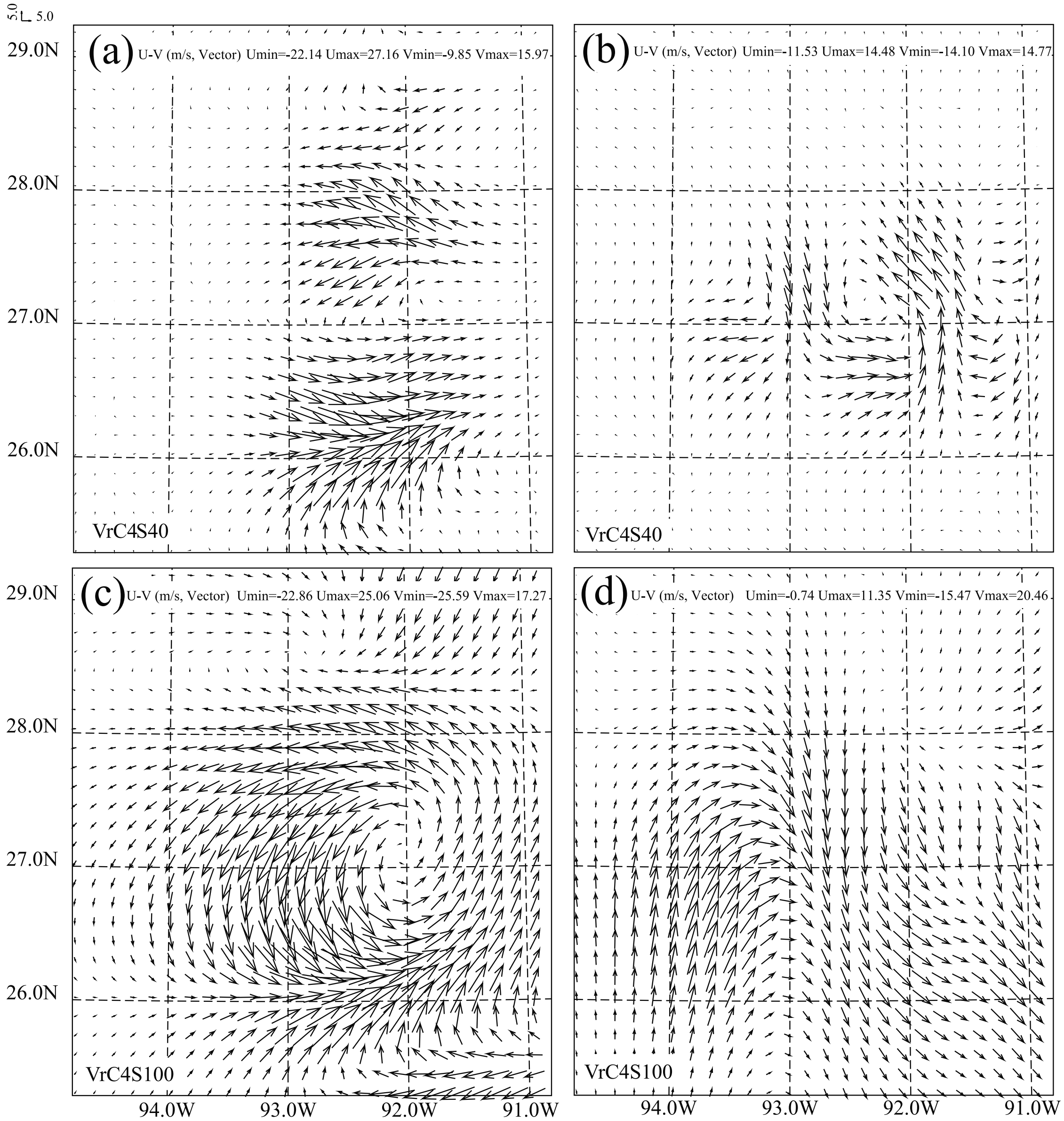

Figure 9. Analyzed increments of wind vectors at 3.5 km height for experiments (a and b) VrC4S40 and (c and d) VrC4S100 from the first (Figures 9a and 9c) and second (Figures 9b and 9d) analysis.

assimilating retrieved winds (ReC4S40, see Group 2 in Table 1). Figure 10 shows the SLP, 25 m AGL wind vectors and speed at 1640 UTC 12 September from CTRL (Figure 10a), ReC4S40 (Figure 10b), and VrC4S40 (Figure 10f), after the final analysis of retrieved winds in ReC4S40 and Vr data in VrC4S40. The H*WIND analysis (Figure 6b) at 1630 UTC 12 September, the closest time to 1640 UTC, shows that the surface maximum wind is located east–northeast of the vortex center. When retrieved wind or Vr data are analyzed, the cyclonic circulation of Ike is strengthened, in particular in the east and northwest regions of the vortex where radar data are available (cf. Figure 2d). ReC4S40 and VrC4S40 increase (decrease) the MSW (minSLP) to about 54 m s^{-1} (956.7 hPa) and 58 m s^{-1} (957.2 hPa), respectively, compared to the 46 m s^{-1} (971 hPa) found in CTRL. The somewhat smaller MSW increase in ReC4S40 is presumably due to the smaller peak velocity values found in retrieved wind data due to smoothing. Overall the improvements to MSW and minSLP in ReC4S40 and VrC4S40 are similar.

[33] Figure 11 shows the SLP, the 25 m AGL wind vectors and speed at 1930 UTC 12 September from CTRL, ReC4S40, and VrC4S40, corresponding to 2 h 50 min forecast time for ReC4S40 and VrC4S40, and 7 h 30 min forecast time for CTRL. With a period of model adjustment, the forecast wind fields are less sensitive to the spatial distribution of wind observations. The available H*WIND analysis at 1930 UTC is shown in Figure 6c. All three experiments produce the MSW northeast of the vortex center, consistent with that in H*WIND analysis (Figure 6c) and forecast similar MSW values which are 41.5 (Figure 11a), 44.1 (Figure 11b), and 41.7 m s^{-1} in CTRL, ReC4S40 and VrC4S40 (Figure 11c), respectively. However, it is apparent that the areas with surface wind speed greater than 40 m s^{-1} are similar in ReC4S40 (Figure 11b) and VrC4S40 (Figure 11c), and are much broader

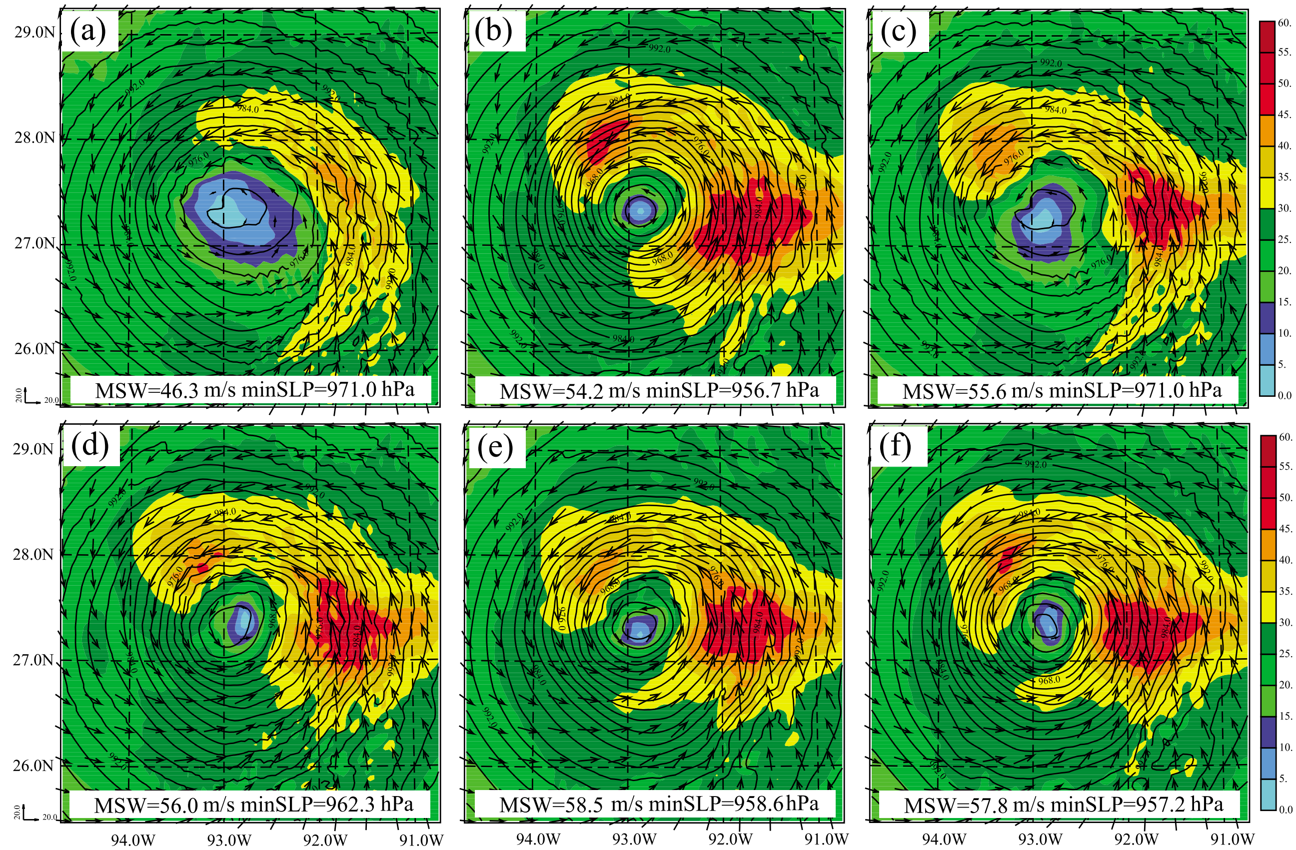

Figure 10. As Figure 5, but for experiments (a) CTRL, (b) ReC4S40, (c) VrC1S40, (d) VrC2S40, (e) VrC3S40, and (f) VrC4S40, after the final analysis at 1640 UTC, 12 September, 2008.

than that in CTRL (Figure 11a). The forecast vortex circulation is strengthened by assimilating ADR wind data (Figure 12a). Also, the forecast minSLP is 958.5 hPa in ReC4S40 and 959.2 hPa in VrC4S40. Compared to the 971.2 hPa in CTRL, they are closer to the 954 hPa in the best track data at 1800 UTC, which is the closest time to 1930 UTC when best track data are available.

[34] Figure 12 compares the forecast tracks and minSLP from CTRL, ReC4S40, and VrC4S40 with the National Hurricane Center (NHC) best track data. It can be seen that the minSLP is more than 15 hPa lower in the radar data assimilation experiments than in CTRL at 1800 UTC 12 September, corresponding to 80 min forecast time for ReC4S40 and VrC4S40, and 6 h forecast time for CTRL, and the pressure remains lower through most of the ensuring 24 h forecast. Table 1 shows that the 24 h mean track errors are 17.8, 18.7, and 26.0 km, for VrC4S40, ReC4S40, and CTRL, respectively, while the mean minSLP errors are 9.2, 8.7, and 15.1 hPa for

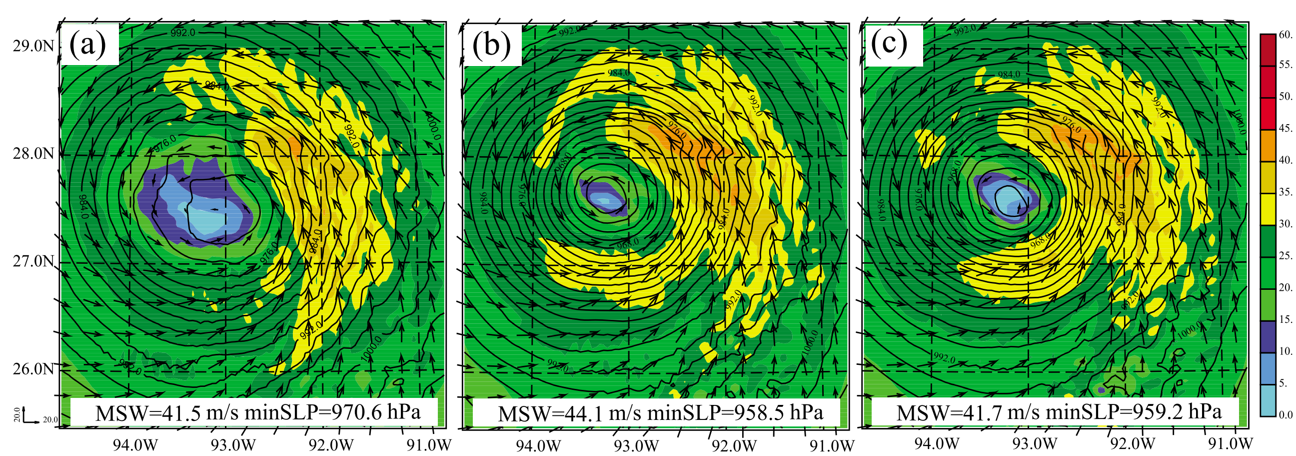

Figure 11. As Figure 5, but for forecasts from experiments (a) CTRL, (b) ReC4S40, and (c) VrC4S40 at 1930 UTC 12 September, 2008.

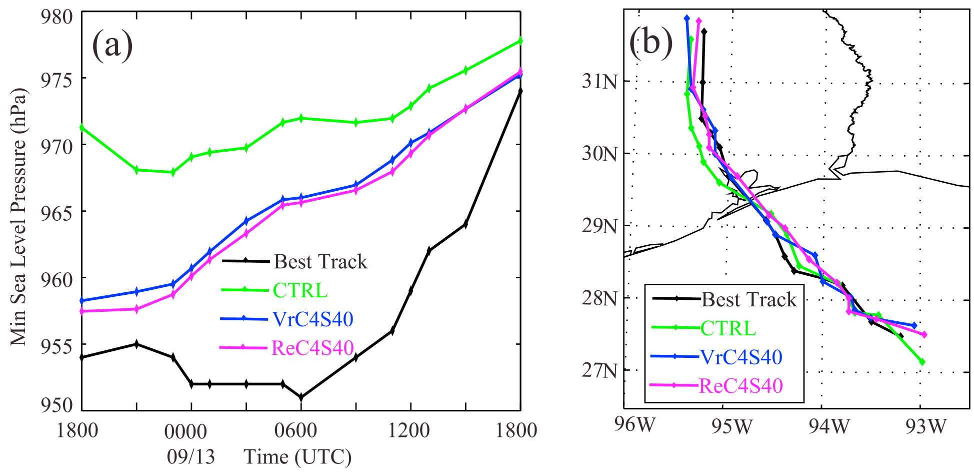

Figure 12. The forecasted (a) minSLPs and (b) tracks from experiments CTRL, ReC4S40, and VrC4S40, during the 24 h forecast period from 1800 UTC, 12 September through 1800 UTC, 13 September, 2008.

the three. The comparisons of predicted MSW from the experiments are not shown because of relatively small systematic differences among the experiments, which are also indicated by the 24 h mean MSW errors in Table 1. Overall, the assimilation of the two types of data result in similar improvements, and the differences are not large enough to say one is better than the other. We also have done experiments assimilating the retrieved winds 1, 2 and 3 times, corresponding to those in Group 3. In all cases, the differences between assimilating Vr data directly and assimilating the retrieved wind data are generally small. These results indicate that Vr data should be assimilated directly with the current 3DVAR procedure. Apart from the additional computational cost for performing pre-retrieval, direct assimilation of Vr data is preferred because they are closer to the original form of measurements. For retrieved data, there is more chance that their errors are correlated and their error characteristics tend to be harder to estimate. Most data assimilation systems, including the ARPS 3DVAR, assume that the observation errors are uncorrelated.

4.3. Impact of Assimilation Cycles

[35] In general, the coverage of ADR data in one flight leg is rather limited (Figure 2). More data sets from different flight legs provide coverage in different parts of the hurricane vortex and reduce the asymmetry of data coverage within the vortex over the period. This inspires us to examine the impact of different number of assimilation cycles on the hurricane prediction. As shown in Figure 4, the experiments labeled C1 through C4 contain 1 through 4 assimilation cycles and the final analysis of all experiments is at 1640 UTC 12 September, around the central time of the last flight leg. These configurations are chosen so that the true initial time of the forecast, defined as the last time when observations are assimilated into the model, is the same. The CTRL experiment has its initial time at 1200 UTC, effectively 4 h 40 min earlier. This is because no GFS analysis is available at the final analysis time. Another reference forecast was generated starting from the GFS analysis at 1800 UTC; forecast results were found to be similar to those of CTRL (not shown).

[36] The analyzed SLP, 25 m AGL wind vectors and speeds at 1640 UTC 12 September from the experiments in Group 3 are shown in Figure 10. Due to the distribution of observations at this time (cf. Figure 2d), near surface wind speed maxima are found east and northwest of the vortex center in all data assimilation experiments, which is not consistent with that shown in Figure 6b. Higher wind speed is increasingly spread over more azimuthal directions as the number of assimilation cycles increases (from 1 in VrC1S40 to 4 in VrC4S40). The overall vortex circulation is also increasingly stronger based on visual inspection of Figure 10, although it is not clearly reflected in the MSW values because the value is dominated by the local maximum in the data dense region east of the vortex center.

[37] There are significant differences in the minSLP among the experiments, however. Without the adjustment to increased wind speed, the minSLP in VrC1S40 (Figure 10c) is 971 hPa, the same as in CTRL (Figure 10a). As the number of cycle increases, the minSLP is reduced to 962.3, 958.6, and 957.2 hPa in VrC2S40, VrC3S40, and VrC4S40, respectively, and the rate of reduction decreases as the number of cycles further increases. The minSLP becomes similar when the number of cycles increases from 3 to 4, which suggests that the benefit of further increasing the number of cycles is being diminished.

[38] As documented in *Berg* [2009], the minSLPs at both 1200 and 1800 UTC 12 September are 954 hPa. Assuming little intensity change between these two times, the minSLP at 1640 UTC can be assumed to be 954 hPa. Obviously, the minSLP of 957.2 hPa in VrC4S40 is the closest to the estimated observation although the minSLP of VrC3S40 is also very similar. The benefits of cycling when analyzing the wind measurements include the continuous adjustment of model state variables to the 'velocity data nudging'. As the vortex circulation is strengthened by the radar wind measurements, the mass field responds the wind to reach a rough gradient wind balance, thereby reducing the vortex central pressure. Convective scale features also develop in response to the strengthened vortex, and to convective scale wind structures introduced by the radar data.

[39] The minSLP values at 1800 UTC, 80 min forecasts after the time of last analysis, are very similar in VrC2S40, VrC3S40 and VrC4S40. They are all significantly improved over that of VrC1S40, and also over CTRL (Figure 13a). In

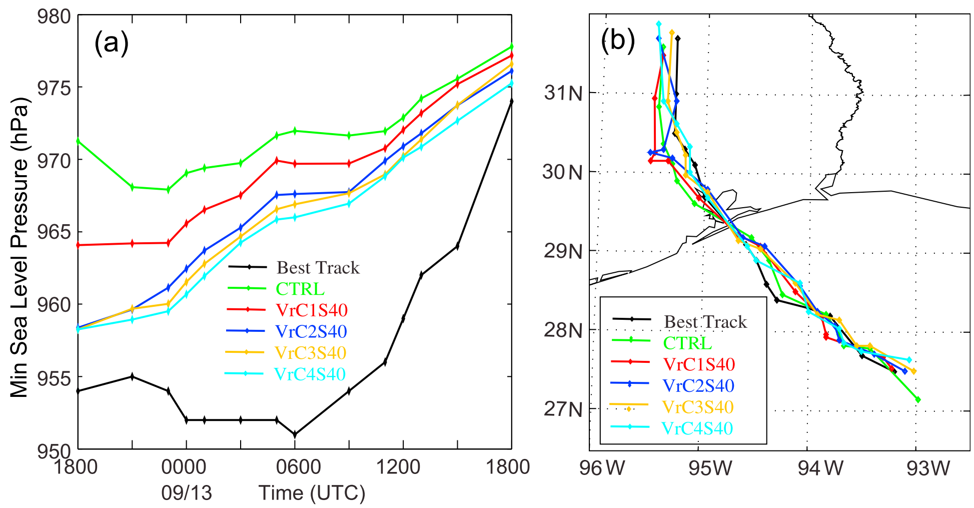

Figure 13. The forecasted (a) minSLPs and (b) tracks from experiments CTRL, VrC1S40, VrC2S40, VrC3S40, and VrC4S40, during the 24 h forecast period from 1800 UTC, 12 September through 1800 UTC, 13 September, 2008.

the ensuring 24 h forecasts, the minSLP in VrC4S40 is the lowest among all experiments. The mean minSLP errors over the 24 h period are 12.8, 10.3, 9.9, and 9.2 hPa for VrC1S40, VrC2S40, VrC3S40, and VrC4S40, respectively, which indicates the accumulative benefits of assimilating more radar data.

[40] Still, among all the experiments examined in this study, none of them is able to capture the intensification of a few hPa between 2100 UTC 12 September and 0000 UTC 13 September. The exact reason is difficult to ascertain; it could be due to insufficient accuracy of the inner core structures in the final analysis that may have been responsible for the intensification, or due to error with the prediction model. A detailed diagnostic analysis is beyond the scope of this study; more observational data will be needed to determine the reason. Latter verification against some independent observations suggests that, at least at the vortex scale, the wind fields in the initial conditions are reasonably accurate. In this study, we are most interested in the relative impact of assimilating the airborne Doppler radar data.

[41] The forecast tracks over the 24 h period for experiments CTRL, VrC1S40, VrC2S40, VrC3S40, and VrC4S40, together with the NHC best track are shown in Figure 13b. Apart from the clearly smaller error at 1800 UTC among the radar assimilation experiments compared to CTRL, the track accuracies at the later forecast hours are similar. Table 1 shows that the 24 h mean track errors are 26, 25.2, 22.2, 18.9, and 17.8 km for CTRL, VrC1S40, VrC2S40, VrC3S40, and VrC4S40, respectively, indicating somewhat greater benefits of assimilating more radar data. In all cases, the 24 h forecast track errors are less than 26 km, which are considered small. The largest impact of assimilating the airborne radar data is clearly on the analyzed hurricane vortex structure and on the short range intensity forecast.

5. Verifications of Analyzed Hurricane Structures and Precipitation Forecasts Near Landfall

[42] As seen from previous discussions, VrC4S40 produces the best analyses of the inner-core structures and hurricane intensity as well as the best intensity and track forecasts. In this section, VrC4S40 is used as the representative example to further illustrate the impact of Vr data on the analyzed hurricane structure and precipitation forecasts near landfall. Independent surface wind speed measurements from a Stepped Frequency Microwave Radiometer (SFMR) carried by the aircraft and the flight-level wind speeds detected by the NOAA P-3 aircraft in-flight measurements are used to verify the analyzed vortex structures.

5.1. Verification of Surface and Flight-Level Wind Speeds

[43] The surface (10 m AGL) wind speeds measured by the airborne SFMR and the flight-level wind speeds detected by the NOAA P-3 aircraft in-flight measurements are plotted in Figures 14 and 15, respectively, along with the corresponding values interpolated from time-dependent model states of VrC4S40 and CTRL for the four flight legs on 12 September, 2008. Clearly, both surface and flight-level wind speeds for all flight legs are much closer to the measurements in VrC4S40 than in CTRL. In Figures 14a and 15a, before 1308 UTC, the solid red curve for VrC4S40 coincides with the dashed green curve for CTRL because the first analysis was run at 1308 UTC; before that time, both are free forecasts from 1200 UTC 12 September. Significant improvements appear after the first assimilation cycle (Figures 14a and 15a). The surface wind minimum is better located and the surface wind profile fits the SFMR observations much better in VrC4S40 than in CTRL. The maximum surface wind speed in VrC4S40 is found at 1319 UTC, very close to the observed time of 1318 UTC, and the speed is about 31 m s^{-1} compared to the observed 38 m s^{-1}. In CTRL, the maximum wind speed is about 29 m s^{-1}, which is found at the end of the flight track, indicating that the model vortex is too large and too weak (Figure 14a). The same can be said about the flight level wind speeds shown in Figure 15a.

[44] In the second fight leg, the wind speeds at both surface (Figure 14b) and flight (Figure 15b) levels in both VrC4S40 and CTRL are close to the observations before the aircraft passes through the vortex center (cf. Figure 2b), although

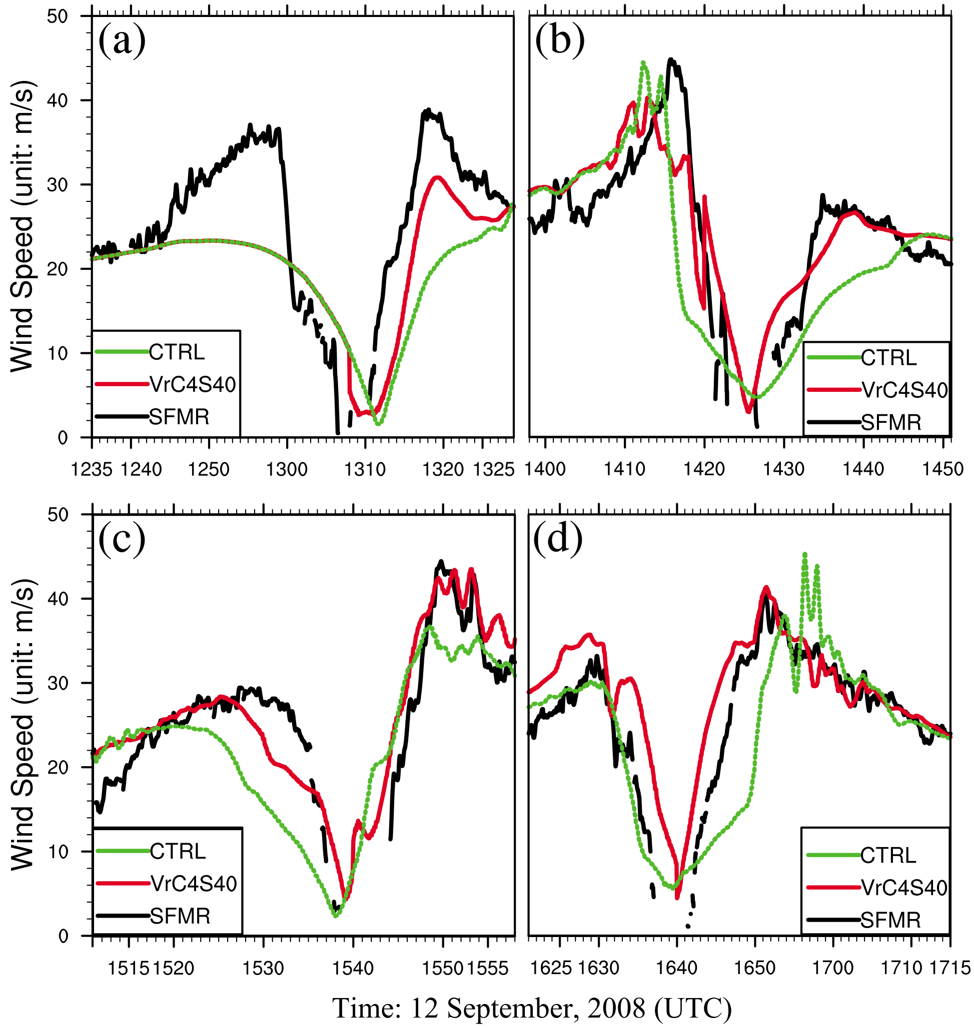

Figure 14. Surface wind speeds along the four flight legs (a) 1235–1329 UTC, (b) 1358–1451 UTC, (c) 1511–1558 UTC, and (d) 1621–1715 UTC, on 12 September, 2008 from the SFMR measurements (black lines), and values interpolated from the time dependent model output of CTRL (green lines) and VrC4S40 (red lines).

CTRL still shows a larger vortex than the observed. After passing through the vortex center, both surface and flight level winds continue to show a much weaker and large vortex in CTRL while the wind profiles in VrC4S40 fit the observations very well. At 1420 UTC when the second analysis is performed, a significant increase is seen in the wind speed profiles at both surface and flight levels (Figure 14b and Figure 15b), and the wind speeds fit the observations better after analysis, especially at flight level where there is better radar data coverage. The next two analyses occur at 1540 and 1640 UTC, close to the time when the aircraft passed through the vortex center. With weak surface winds near the vortex center, the adjustment to the surface wind speed profiles at the last two analyses time are smaller than that at the first two analyses time (Figures 14c and 14d), although the adjustment at flight level is still significant (Figures 15c and 15d). The fourth analysis correctly reduces the flight-level wind speeds near the center (Figure 15d), but the third analysis incorrectly increases the wind speeds near the wind speed minimum (Figure 15c). Because of the very large wind speed gradient in the vortex core region, a small spatial displacement of the background or analyzed vortex can cause such an error. Still, overall, the wind profiles at both times fit the observed flight tracks very well, much better than those in CTRL, and the fit to observations generally improves as the number of assimilation cycle increases.

[45] Taking the fourth flight leg as an example (Figure 14d), the two peak surface wind speeds are placed rather accurately at around 1630 and 1650 UTC (which in space are at the correct radii). The peak wind speed near 1650 UTC, after the fourth analysis, fits the observed profile especially well, with speed and timing errors being less than 1 m s^{-1} and 1 min, respectively. A similar result is found with the flight level wind profile shown in Figure 15d, after the fourth analysis.

[46] The mean biases and RMS errors of surface and flight-level wind speeds averaged over all four flight legs (Table 2) are calculated against the SFMR and fight-level observations. The mean biases in VrC4S40 are -0.2 m s^{-1} (surface) and -2.2 m s^{-1} (flight level), much smaller than the -3.6 m s^{-1} (surface) and -7.0 m s^{-1} (flight level) of CTRL. The mean RMS errors in VrC4S40 are 4.1 m s^{-1}

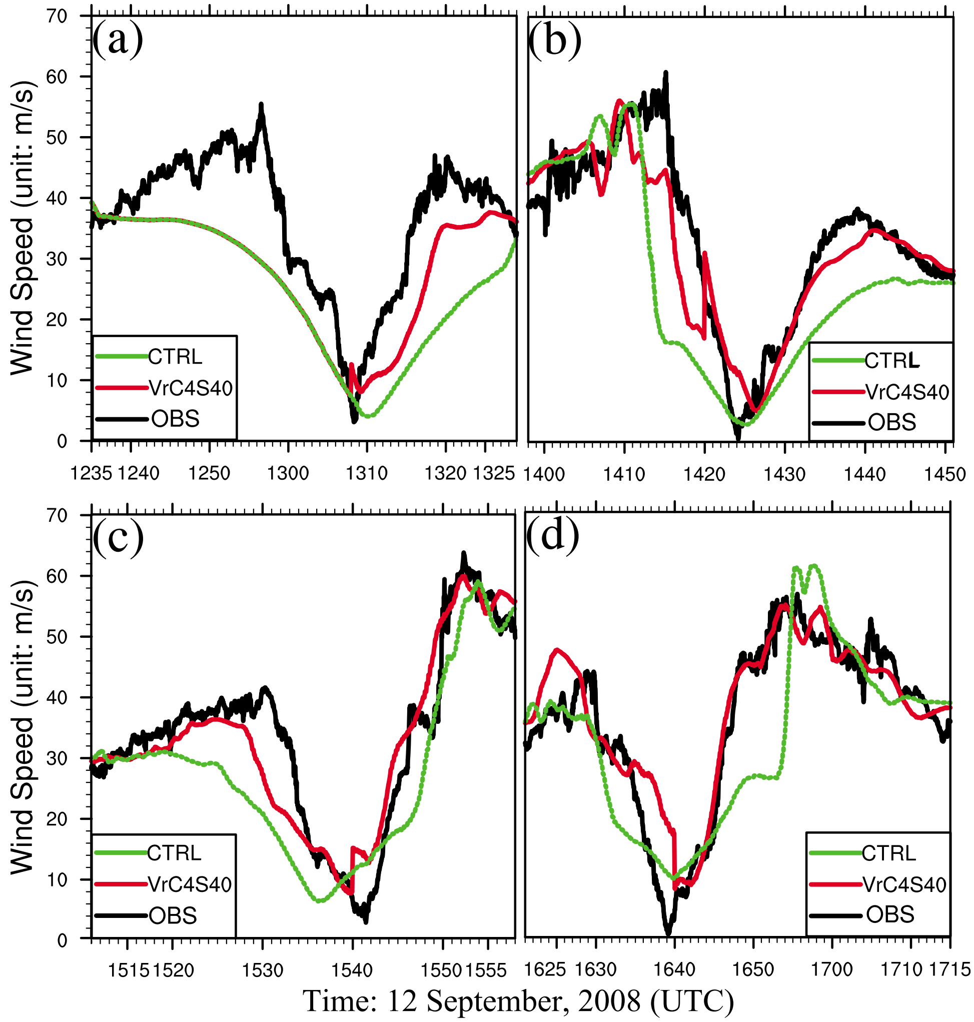

Figure 15. As Figure 13 but for flight-level wind speeds.

(surface) and 5.3 m s^{-1} (flight level), smaller than the 5.8 m s^{-1} (surface) and 8.6 m s^{-1} (flight level) of CTRL. Given that the SFMR and flight-level wind data are independent observations that were not used in the data assimilation, the results indicate that the assimilation of airborne Doppler radar radial velocity data is effective in establishing accurate hurricane vortex circulations, and that the vortex circulations in both the analyses and short-range forecasts improve as more data are assimilated through the intermittent assimilation cycles.

5.2. Structure Verification

[47] Figure 16 presents the SLP and surface wind vectors and speed from experiments CTRL and VrC4S40, at 0700 UTC 13 September, 2008, the time of Hurricane Ike landfall at the Texas coast. The H*WIND analysis at 0730 UTC 13 September (Figure 6d), the nearest time to 0700 UTC, shows that the surface maximum wind is again located east–northeast of the vortex center. Even though the forecasts of VrC4S40 and CTRL also place the maximum wind east–northeast of the vortex center, the predicted wind structures exhibit considerable differences. The region with wind speed higher than 30 m s^{-1} is larger in VrC4S40 than in CTRL. VrC4S40 also predicts tighter inner-core vortex circulations with a smaller radius of MSW, although the values of MSW are very close between CTRL (34.2 m s^{-1}) and VrC4S40 (35.0 m s^{-1}). The forecast SLPs at this time are quite different between CTRL and VrC4S40. The minSLPs of CTRL and VrC4S40 are 971.9 hPa (Figure 16a) and 966.3 hPa (Figure 16b), respectively. The best track minSLP is 951 hPa at 0600 UTC 13 September (an hour before landfall) and 954 hPa at 0900 UTC (Figure 13a). VrC4S40 therefore has a better SLP forecast than CTRL does at landfall. In summary, experiment VrC4S40, which assimilated airborne Vr data in 4 cycles about 14 h earlier, forecasts a stronger and tighter vortex at the time of landfall, although its intensity is still weaker than the observation. Other experiments assimilating radar data

Table 2. The Mean Biases and RMS Errors of Surface and flight-Level Wind Speeds Averaged Over All Four Flight Legs for CTRL and VrC4S40

Experiment	Height	Mean Bias (m s^{-1})	Mean RMSE (m s^{-1})
CTRL	Surface	−3.6	5.8
	Flight level	−7.0	8.6
VrC4S40	Surface	−0.2	4.1
	Flight Level	−2.2	5.3

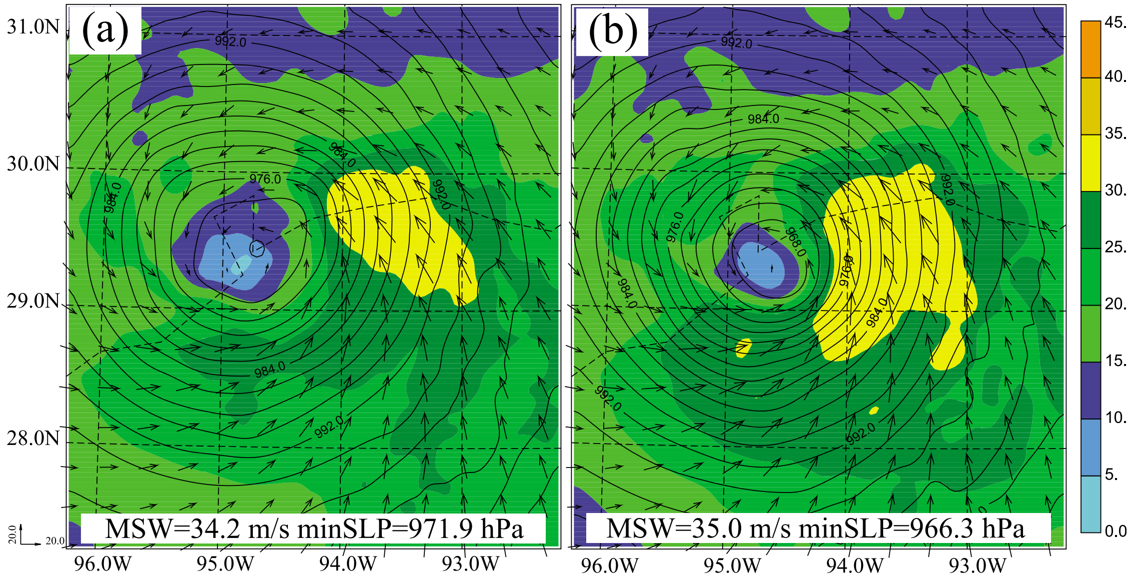

Figure 16. Similar to Figure 5, except that they are for experiments (a) CTRL and (b) VrC4S40 at 0700 UTC 13 September, 2008, the time of Hurricane Ike landfall at the Texas coast.

also predict a stronger vortex at the landfall time than CTRL does, with VrC4S40 predicting the strongest one (cf. Figure 13a).

5.3. Precipitation Verification

[48] Figure 17 shows the total accumulated precipitation during the 24 h forecast period starting from 1800 UTC 12 September, 2008, from CTRL and VrC4S40 along with the corresponding NCEP 4-km-resolution Stage IV precipitation analysis [*Lin and Mitchell*, 2005]. Over the ocean, the Stage IV precipitation analysis is mostly based on radar precipitation estimates, and the absence of precipitation south of 28N is due to the lack of coastal radar data coverage. More precipitation is found to extend further southeast over the ocean in both CTRL (Figure 17b) and VrC4S40 (Figure 17c) compared to the observations (Figure 17a). In general, the strongest precipitation is found near the coast, with the observed heavy precipitation extending further inland (Figure 17a) than the model predictions (Figures 17b and 17c). Right at the coast, both VrC4S40 and CTRL predict heavy precipitation exceeding 100 mm, but the precipitation to the north is too weak. Between VrC4S40 and CTRL, the former predicts more precipitation. The aerial coverage of 50 mm accumulated precipitation in VrC4S40 (Figure 17c) is much closer to the observation than that in CTRL (Figure 17b). The equitable threat score (ETS) for this 50 mm threshold is 0.44 for VrC4S40 (Figure 17c), which is higher than 0.34 for CTRL (Figure 17b). Other ADR data assimilation experiments result in similar though somewhat smaller improvements (not shown).

6. Summary and Conclusions

[49] In this study, the ability to analyze radial velocity data from airborne Doppler radar is added to the ARPS 3DVAR data assimilation system. Unlike ground-based Doppler

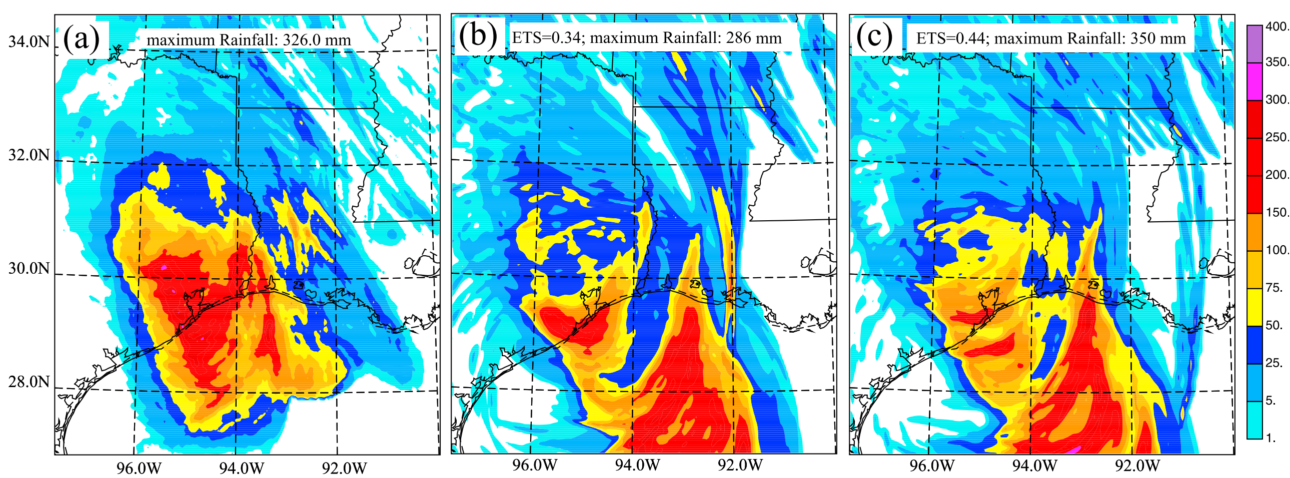

Figure 17. The 24 h accumulated precipitation (mm) valid at 1800 UTC 13 September, 2008 from (a) NCEP Stage IV precipitation analyses, and forecasts of (b) CTRL, and (c) VrC4S40. The equitable threat scores of 24 h accumulated precipitation for the 50-mm threshold are shown for the experiments.

radar data that are first mapped to the model grid points for ARPS 3DVAR, the airborne radar data are kept on the radial beams. The radial velocity observation operator involves spatial interpolation of velocity components on the model grid points to the observation points, and the projection of the velocity to the radial directions. Because the airborne radar is constantly moving, each radial beam has its own radar position. Superobbing is performed in the radial direction by averaging 30 range gates at 150 m intervals to arrive at a radial resolution comparable to the analysis grid resolution (4 km grid spacing). The enhanced 3DVAR system is applied to the assimilation of airborne radar data collected along four flight legs through Hurricane Ike (2008), 14 to 18 h before it made landfall.

[50] A few existing studies examining the impact of airborne radar wind data on tropical cyclone prediction using a 3DVAR method (from the WRF system) have assimilated pre-retrieved wind components from the radial velocity data. In this study, a comparison is made between assimilating the retrieved winds and assimilating the radial velocity data directly using the ARPS 3DVAR. The ARPS 3DVAR employs a Gaussian background error correlation model; a set of sensitivity experiments is first performed to determine the optimal horizontal error de-correlation scale. The effect of assimilation cycles is also examined. Evaluations are made based on intensity and track predictions for Ike within a 24 h period as compared to best track data. The analyzed and predicted surface wind speeds are compared with available operational H*WIND analyses. Verifications against independent surface wind speed measurements from an airborne stepped frequency microwave radiometer and against independent flight-level wind speed measurements are also made during the assimilation cycles. The predicted hurricane vortex structure and intensity at the landfall time are also examined and 24 h accumulated precipitation forecast is verified against the NCEP Stage IV rainfall estimate. The main conclusions are as follows.

[51] 1. Clear positive impacts on the analysis and prediction of Hurricane Ike are found, which are from assimilating airborne radar velocity data. This conclusion is consistent with a few recently published studies although earlier studies using a 3DVAR method have only assimilated pre-retrieved velocity components.

[52] 2. Given the non-uniform spatial coverage of the airborne Doppler radar data, the analysis and forecast are found to be moderately sensitive to the choice of the horizontal background error de-correlation scale. A value of 40 km is found to produce the best prediction of track and intensity for Hurricane Ike. This optimal value may or may not be case and grid configuration dependent.

[53] 3. The assimilation of retrieved horizontal wind components and of original radial velocity data produces similar results in two inter-comparison experiments. This is not too surprising because the retrieved winds were produced using a 3DVAR method similar to the ARPS 3DVAR, except that the latter is more general and is performed directly on the terrain-following model grid. Theoretically, assimilating radial velocity data directly is advantageous. Practically, performing the pre-retrieval carries additional computational cost, and delays real-time data assimilation operations. It is therefore recommended that the radial velocity data are directly assimilated, after proper quality control.

[54] 4. The assimilation of radial velocity observations from all four flight legs through intermittent assimilation cycles produces the best analyses and forecasts, better than when data from some of the four legs are used. Because of large error in the vortex intensity in the GFS analysis background, the first analysis tends to produce the largest analysis increment. It is through mutual adjustments among model variables during the forecast periods that a balanced vortex with lowered center pressure is established.

[55] 5. Verification of surface and flight-level wind speeds extracted from the assimilated model state against independent SFMR and flight-level wind data showed excellent agreement, and the fit of the model state to observations improves as more radar data are assimilated.

[56] 6. The best-analyzed hurricane with radar data assimilation was about 4 hPa too weak and it remained too weak during the forecast period. This problem with the analyzed hurricane being too weak in terms of minimum central pressure is also found by *Zhao and Xue* [2009] when only radial velocity data from two coastal radars are assimilated. The same thing happens when the more sophisticated EnKF method is used in *Dong and Xue* [2012]. Assimilating best track minimum surface pressure data using the EnKF has been found to be very helpful for Ike [*Dong*, 2010] but not so when it is analyzed by the univariate ARPS 3DVAR for a typhoon case [*Zhao et al.*, 2012b]. All forecasts missed the slight intensification phase 4 to 7 h into the forecasts, and model errors as well as initial condition errors may be the cause but the exact reason will require further investigation.

[57] 7. At the time of landfall, Hurricane Ike is somewhat stronger and closer to observed intensity in the radar data assimilation experiments than the experiment without radar data assimilation. The 24 h accumulated precipitation greater than 50 mm from VrC4S40 is noticeably improved over the case without radar data assimilation, although forecast precipitation inland is weaker than observed overall.

[58] Finally we note that the results presented in this paper are based on a single case, when the hurricane was in a weakening stage that also includes a period after landfall during the forecast. For more robust conclusions on the impact of airborne Doppler radar velocity data, more cases should be examined, and for different stages of hurricane life cycles. The optimal horizontal de-correlation scale determined in this study may need further experimentation in other cases, and methods that better account for timing differences among the observations collected within the flight legs can be used to further improve the analysis accuracy. For the latter, the 'first guess at the appropriate time (FGAT)' method can be used with a 3DVAR method [e.g., *Buehner et al.*, 2010] while in the ensemble Kalman filter context four dimensional extensions can be implemented [e.g., *Hunt et al.*, 2004; *Wang et al.*, 2012]. With more advanced data assimilation methods, the impact of airborne radar data is likely to be even greater. In addition, the GBVTD method successfully used in *Zhao et al.* [2012a] to initialize a typhoon may be beneficial for assimilating airborne radar data which tend to the asymmetric azimuthal coverage. These can be topics for future research.

[59] **Acknowledgments.** This work was primarily supported by the Office of Naval Research grants N00014-10-1-0775, N00014-10-1-0133, NSF grants AGS-0802888 and OCI-0905040, and grant KLME060203 from NUIST. Ming Xue was also supported by NSF grants AGS-0750790, AGS-

0941491, AGS-1046171, and AGS-1046081. Assistance from John Gamache of NOAA/AOML/HRD with the use of airborne radar data is greatly appreciated. Help from K. Brewster, J. Gao, and Y. Wang for using data, software, ARPS and ARPS 3DVAR is also acknowledged. The comments on our initial draft by F. Kong are greatly acknowledged. J. Schleif is thanked for proofreading the manuscript. Q. Wang, J. Dong and K. Zhu are thanked for their help with our experiments. Computations were performed on supercomputer Ranger of TACC operated by the University of Texas.

References

Berg, R. (2009), Tropical Cyclone Report: Hurricane Ike, 1–14 September 2008, report, 25 pp., Natl. Hurricane Cent., Miami, Fla. [Available at http://www.nhc.noaa.gov/pdf/TCR-AL092008_Ike.pdf.]

Blackwell, K. G. (2000), The evolution of Hurricane Danny (1997) at landfall: Doppler-observed eyewall replacement, vortex contraction/intensification, and low-level wind maxima, *Mon. Weather Rev.*, *128*, 4002–4016, doi:10.1175/1520-0493(2000)129<4002:TEOHDA>2.0.CO;2.

Brewster, K., M. Hu, M. Xue, and J. Gao (2005), Efficient assimilation of radar data at high resolution for short-range numerical weather prediction, paper presented at International Symposium on Nowcasting and Very Short Range Forecasting, WMO, Geneva, Switzerland.

Buehner, M., P. L. Houtekamer, C. Charette, H. L. Mitchell, and B. He (2010), Intercomparison of variational data assimilation and the ensemble Kalman filter for global deterministic NWP. Part II: One-month experiments with real observations, *Mon. Weather Rev.*, *138*, 1567–1586, doi:10.1175/2009MWR3158.1.

Davis, C., et al. (2008), Prediction of landfalling hurricanes with the Advanced Hurricane WRF Model, *Mon. Weather Rev.*, *136*, 1990–2005, doi:10.1175/2007MWR2085.1.

Dong, J. (2010), Applications of ensemble Kalman filter data assimilation: From convective thunderstorms to hurricanes, PhD dissertation, 199 pp., Univ. of Okla., Norman.

Dong, J., and M. Xue (2012), Assimilation of radial velocity and reflectivity data from coastal WSR-88D radars using ensemble Kalman filter for the analysis and forecast of landfalling Hurricane Ike (2008), *Q. J. R. Meteorol. Soc.*, doi:10.1002/qj.1970, in press.

Elsberry, R. L. (2005), Achievement of USWRP Hurricane Landfall Research Goal, *Bull. Am. Meteorol. Soc.*, *86*, 643–645, doi:10.1175/BAMS-86-5-643.

Gamache, J. F. (2005), Real-time dissemination of hurricane wind fields determined from airborne Doppler radar, JHT Project final report, 38 pp., Natl. Hurricane Cent., Miami, Fla. [Available at http://www.nhc.noaa.gov/jht/2003-2005reports/DOPLRgamache_JHTfinalreport.pdf.]

Gamache, J. F., J. S. Griffin, P. P. Dodge, and N. F. Griffin (2004), Automatic Doppler analysis of three-dimensional wind fields in hurricane eyewalls, paper presented at 26th Conference on Hurricanes and Tropical Meteorology, Am. Meteorol. Soc., Miami, Fla.

Gao, J.-D., M. Xue, A. Shapiro, and K. K. Droegemeier (1999), A variational method for the analysis of three-dimensional wind fields from two Doppler radars, *Mon. Weather Rev.*, *127*, 2128–2142, doi:10.1175/1520-0493(1999)127<2128:AVMFTA>2.0.CO;2.

Gao, J.-D., M. Xue, K. Brewster, and K. K. Droegemeier (2004), A three-dimensional variational data analysis method with recursive filter for Doppler radars, *J. Atmos. Oceanic Technol.*, *21*, 457–469, doi:10.1175/1520-0426(2004)021<0457:ATVDAM>2.0.CO;2.

Houze, R. A., Jr., S. S. Chen, B. F. Smull, W.-C. Lee, and M. M. Bell (2007), Hurricane intensity and eyewall replacement, *Science*, *315*, 1235–1239, doi:10.1126/science.1135650.

Hu, M., and M. Xue (2007), Impact of configurations of rapid intermittent assimilation of WSR-88D radar data for the 8 May 2003 Oklahoma City tornadic thunderstorm case, *Mon. Weather Rev.*, *135*, 507–525, doi:10.1175/MWR3313.1.

Hu, M., M. Xue, and K. Brewster (2006a), 3DVAR and cloud analysis with WSR-88D level-II data for the prediction of Fort Worth tornadic thunderstorms. Part I: Cloud analysis and its impact, *Mon. Weather Rev.*, *134*, 675–698, doi:10.1175/MWR3092.1.

Hu, M., M. Xue, J. Gao, and K. Brewster (2006b), 3DVAR and cloud analysis with WSR-88D level-II data for the prediction of Fort Worth tornadic thunderstorms. Part II: Impact of radial velocity analysis via 3DVAR, *Mon. Weather Rev.*, *134*, 699–721, doi:10.1175/MWR3093.1.

Hunt, B. R., E. Kalnay, E. J. Kostelich, E. Ott, D. J. Patil, T. Sauer, I. Szunyogh, J. A. York, and A. V. Zimin (2004), Four-dimensional ensemble Kalman filtering, *Tellus, Ser. A*, *56*, 273–277.

Kalnay, E. (2002), *Atmospheric Modeling, Data Assimilation, and Predictability*, 341 pp., Cambridge Univ. Press, Cambridge, U. K., doi:10.1017/CBO9780511802270.

Li, Y., X. Wang, and M. Xue (2012), Assimilation of radar radial velocity data with the WRF ensemble-3DVAR hybrid system for the prediction of Hurricane Ike (2008), *Mon. Weather Rev.*, doi:10.1175/MWR-D-12-00043.1, in press.

Lin, Y., and K. E. Mitchell (2005), The NCEP Stage II/IV hourly precipitation analyses: Development and applications, paper presented at 19th Conference on Hydrology, Am. Meteorol. Soc., San Diego, Calif.

Lin, Y.-L., R. D. Farley, and H. D. Orville (1983), Bulk parameterization of the snow field in a cloud model, *J. Clim. Appl. Meteorol.*, *22*, 1065–1092, doi:10.1175/1520-0450(1983)022<1065:BPOTSF>2.0.CO;2.

Marks, F. D., Jr., and R. A. Houze Jr. (1984), Airborne Doppler radar observations in Hurricane Debby, *Bull. Am. Meteorol. Soc.*, *65*, 569–582, doi:10.1175/1520-0477(1984)065<0569:ADROIH>2.0.CO;2.

Marks, F. D., Jr., and R. A. Houze Jr. (1987), Inner-core structure of Hurricane Alicia from airborne Doppler radar observations, *J. Atmos. Sci.*, *44*, 1296–1317, doi:10.1175/1520-0469(1987)044<1296:ICSOHA>2.0.CO;2.

Powell, M. D., S. H. Houston, L. R. Amat, and N. Morisseau-Leroy (1998), The HRD real-time hurricane wind analysis system, *J. Wind Eng. Ind. Aerodyn.*, *77–78*, 53–64, doi:10.1016/S0167-6105(98)00131-7.

Pu, Z., X. Li, and J. Sun (2009), Impact of airborne Doppler radar data assimilation on the numerical simulation of intensity changes of hurricane Dennis near a landfall, *J. Atmos. Sci.*, *66*, 3351–3365, doi:10.1175/1009JAS3121.1.

Reasor, P. D., M. T. Montgomery, F. D. Marks, and J. F. Gamache (2000), Low-wavenumber structure and evolution of the hurricane inner core observed by airborne dual-Doppler radar, *Mon. Weather Rev.*, *128*, 1653–1680, doi:10.1175/1520-0493(2000)128<1653:LWSAEO>2.0.CO;2.

Schenkman, A., M. Xue, A. Shapiro, K. Brewster, and J. Gao (2011), The analysis and prediction of the 8–9 May 2007 Oklahoma tornadic mesoscale convective system by assimilating WSR-88D and CASA radar data using 3DVAR, *Mon. Weather Rev.*, *139*, 224–246, doi:10.1175/2010MWR3336.1.

Skamarock, W. C., J. B. Klemp, J. Dudhia, D. O. Gill, D. M. Barker, W. Wang, and J. D. Powers (2005), A Description of the Advanced Research WRF Version 2, report, 88 pp., NCAR, Boulder, Colo.

Uhlhorn, E. W., and P. G. Black (2003), Verification of remotely sensed sea surface winds in hurricanes, *J. Atmos. Oceanic Technol.*, *20*, 99–116, doi:10.1175/1520-0426(2003)020<0099:VORSSS>2.0.CO;2.

Wang, S., M. Xue, and J. Min (2012), A four-dimensional asynchronous ensemble square-root filter (4DEnSRF) and tests with simulated radar data, *Q. J. R. Meteorol. Soc.*, doi:10.1002/qj.1987, in press.

Weng, Y., and F. Zhang (2012), Assimilating airborne Doppler radar observations with an ensemble Kalman filter for convection-permitting hurricane initialization and prediction: Katrina (2005), *Mon. Weather Rev.*, *140*, 841–859, doi:10.1175/2011MWR3602.1.

Xiao, Q., Y.-H. Kuo, J. Sun, W.-C. Lee, D. M. Barker, and E. Lim (2007), An approach of radar reflectivity data assimilation and its assessment with the inland QPF of typhoon Rusa (2002) at landfall, *J. Appl. Meteorol. Climatol.*, *46*, 14–22, doi:10.1175/JAM2439.1.

Xiao, Q., X. Zhang, C. Davis, J. Tuttle, G. Holland, and P. J. Fitzpatrick (2009), Experiments of hurricane initialization with airborne Doppler radar data for the Advanced Research Hurricane WRF (AHW) model, *Mon. Weather Rev.*, *137*, 2758–2777, doi:10.1175/2009MWR2828.1.

Xue, M., K. K. Droegemeier, V. Wong, A. Shapiro, and K. Brewster (1995), *ARPS Version 4.0 User's Guide*, 380 pp., CAPS, Univ. of Okla., Norman. [Available at http://www.caps.ou.edu/ARPS.]

Xue, M., K. K. Droegemeier, and V. Wong (2000), The Advanced Regional Prediction System (ARPS)—A multiscale nonhydrostatic atmospheric simulation and prediction tool. Part I: Model dynamics and verification, *Meteorol. Atmos. Phys.*, *75*, 161–193, doi:10.1007/s007030070003.

Xue, M., K. K. Droegemeier, V. Wong, A. Shapiro, K. Brewster, F. Carr, D. Weber, Y. Liu, and D. Wang (2001), The Advanced Regional Prediction System (ARPS)—A multi-scale nonhydrostatic atmospheric simulation and prediction tool. Part II: Model physics and applications, *Meteorol. Atmos. Phys.*, *76*, 143–165, doi:10.1007/s007030170027.

Xue, M., D.-H. Wang, J.-D. Gao, K. Brewster, and K. K. Droegemeier (2003), The Advanced Regional Prediction System (ARPS), storm-scale numerical weather prediction and data assimilation, *Meteorol. Atmos. Phys.*, *82*, 139–170, doi:10.1007/s00703-001-0595-6.

Zhang, F., Y. Weng, J. F. Gamache, and F. D. Marks (2011), Performance of convection-permitting hurricane initialization and prediction during 2008–2010 with ensemble data assimilation of inner-core airborne Doppler radar observations, *Geophys. Res. Lett.*, *38*, L15810, doi:10.1029/2011GL048469.

Zhao, K., and M. Xue (2009), Assimilation of coastal Doppler radar data with the ARPS 3DVAR and cloud analysis for the prediction of Hurricane Ike (2008), *Geophys. Res. Lett.*, *36*, L12803, doi:10.1029/2009GL038658.

Zhao, K., M. Xue, and W.-C. Lee (2012a), Assimilation of GBVTD-retrieved winds from single-Doppler radar for short-term forecasting of

Super Typhoon Saomai (0608) at landfall, *Q. J. R. Meteorol. Soc.*, *138*, 1055–1071, doi:10.1002/qj.1975.
Zhao, K., X. Li, M. Xue, B. J.-D. Jou, and W.-C. Lee (2012b), Short-term forecasting through intermittent assimilation of data from Taiwan and mainland China coastal radars for Typhoon Meranti (2010) at landfall, *J. Geophys. Res.*, *117*, D06108, doi:10.1029/2011JD017109.
Zhao, Q. Y., and Y. Jin (2008), High-resolution radar data assimilation for Hurricane Isabel (2003) at landfall, *Bull. Am. Meteorol. Soc.*, *89*, 1355–1372, doi:10.1175/2008BAMS2562.1.